Doxorubicin accelerates and enhances rAAV-mediated gene expression in the cortex of mouse, cat and monkey

Hongliang Gong[1,2], Nini Yuan[1], Zhiming Shen[1], Cheng Tang[1,2], Stewart Shipp[1], Liling Qian[1], Yiliang Lu[1], Ian Max Andolina[1], Shenghai Zhang[4], Jihong Wu[4*], Hui Yang[1,2,3*], Wei Wang[1,2,3*]

[1]Institute of Neuroscience, the Center for Excellence in Brain Science and Intelligence Technology, State Key Laboratory of Neuroscience, Key Laboratory of Primate Neurobiology, Chinese Academy of Sciences, Shanghai 200031, China

[2]University of Chinese Academy of Sciences, Beijing 100049, China

[3]Shanghai Center for Brain and Brain-Inspired Intelligence Technology, Shanghai 200031, China

[4]Department of Ophthalmology, Eye and ENT Hospital of Fudan University, Shanghai 200031, China

*Correspondence to: w.wang@ion.ac.cn; jihongwu@fudan.edu.cn; huiyang@ion.ac.cn

Abstract

Rapid and efficient gene transduction via recombinant adeno-associated viruses (rAAVs) is highly desirable across many basic and clinical research domains. Here we report that vector co-infusion with doxorubicin, a clinical anti-cancer drug, markedly enhanced rAAV-mediated gene expression in the cerebral cortex across mammalian species (cat, mouse, and macaque), acting throughout the time-period examined and detectable at just three days post-transfection. This enhancement showed serotype generality, being common to tested rAAV serotypes 2, 8, 9 and PHP.eB, and was observed both locally, and at remote locations consistent with doxorubicin undergoing retrograde axonal transport. All these effects were observed at doses matching human blood plasma levels in clinical therapy, and lacked detectable cytotoxicity as assessed by cell morphology, activity, apoptosis and behavioral testing. Altogether, this study identifies an effective means to improve the capability and scope of *in vivo* rAAV applications, accelerating and augmenting gene transduction at doxorubicin concentrations paralleling medical practice.

Introduction

Having a potent capability for safe and stable transduction, recombinant adeno-associated virus (rAAV) are favored for *in vivo* gene delivery in mammalian central nervous system (CNS), e.g. for such purposes as gene editing and expression modulation (Atasoy et al., 2008; Ran et al., 2015), neuronal morphology mapping (Parekh and Ascoli, 2013), *in vivo* imaging (Tian et al., 2009), neural circuit analysis (Cruz-Martin et al., 2014; Zhang et al., 2016) and treatment of neurological disorders (Hudry and Vandenberghe, 2019). However, the expression of genes transduced via rAAV undergoes a

prolonged lag phase before reaching significant levels for intervention (≥ two weeks) (Diester et al., 2011; Ju et al., 2018). This delay in expression limits the utility of rAAV applications in both experimental and clinical practice, especially in neurodevelopmental studies (Krol and Feng, 2018) and disease treatments that require timely intervention to forestall irreversible tissue damage (e.g., ischemic brain injury)(Shimazaki et al., 2000). Thus a more effective means to induce rapid and high-level rAAV-based transgene expression in mammalian CNS is in much need of development.

Previous research efforts have aimed to improve the vector system, i.e. the viral capsid and genome. By utilizing natural isolates with different tropisms, new rAAV variants with superior efficacy have been engineered through capsid transformation (Broekman et al., 2006), amino acid mutation (Zhong et al., 2008), domain/ subunit swapping (Rabinowitz et al., 2004), or screened from mutant capsid libraries (Deverman et al., 2016; Maheshri et al., 2006; Yang et al., 2009). At the level of vector genome, the vector expression cassette has been optimized with stronger promoters, enhancers, and more effective polyadenylation sequences (Peel et al., 1997; Wang et al., 2019). By modifying one of the inverted terminal repeats (ITR), self-complementary AAV (scAAV) has been generated to bypass second-strand synthesis to improve the efficacy of transduction (McCarty et al., 2003). Combined with advances in delivery techniques, good progress has been achieved in respect of transduction efficiency in small animals (Chan et al., 2017). However, for large mammals represented by non-human primates and humans, it remains challenging to achieve consistent, high levels of transduction across volumetrically extensive brain structures. This problem is manifest in both therapeutic trials and research applications (Hadaczek et al., 2010; Hwu et al., 2012), enforced by capsid specific cytotoxic T lymphocyte response (Mingozzi et al., 2007). Furthermore, the delay in expression remains critically important, since scAAV can only be used for smaller transgenes (less than 2.2 kb)(Wang et al., 2019).

The application of exogenous agents is a new strategy to promote rAAV transduction in the CNS. Early studies revealed that techniques such as ionizing radiation and genotoxic agents can promote rAAV2 transduction, inducing faster and higher transgene expression in cultured cells (Fisher et al., 1996; Kanazawa et al., 2001). Similar promotion was achieved with chemical agents that damage DNA, inhibit topoisomerase activity, or modulate proteasome function (Nicolson et al., 2016; Russell et al., 1995; Yan et al., 2004). These agents appear to promote viral intracellular trafficking or second-strand DNA synthesis, two rate-limiting steps in the process of rAAV transduction that see little improvement with vector capsid engineering. However, severe side-effects have hindered their application *in vivo,* calling for alternative drugs or strategies that are less cytotoxic. ***Doxorubicin*** is a frontline drug that has been widely used in cancer therapy (Tacar et al., 2013). As a known inhibitor of topoisomerase and proteasome (Sishi et al., 2013; Tacar et al., 2013), it has clear potential to promote rAAV transduction, as evidenced by application to cultured cells (Yan et al., 2004; Zhang et al., 2012; Zhang et al., 2009). However, to pave the way for incorporation of doxorubicin in rAAV

protocols for CNS, it is essential to examine the precise time-course of neural transduction, and the dose-dependency of the long-term balance between efficacy and neurotoxicity. It was thus our goal to determine how effectively doxorubicin might accelerate rAAV-mediated gene transduction in mammalian CNS and establish the ceiling for toxicity. Furthermore, it is imperative to determine the universality of the action of doxorubicin across a range rAAV serotypes, brain structures, and mammalian species.

Here, we have systematically evaluated the effect of doxorubicin on transgene expression in the cerebral cortex of mice, cats, and macaque monkeys, by intraparenchymal administration of doxorubicin in combination with different rAAV serotypes (rAAV8, rAAV2, rAAV9 and rAAV-PHP.eB). We found that doxorubicin greatly enhanced local transgene expression mediated by every rAAV vector that was tested, differing little between species. Across subjects, doxorubicin took almost immediate effect and continued to act throughout the time period examined. Dose escalation testing showed that the effect of doxorubicin on rAAV transduction was concentration-dependent, and was mediated with negligible adverse side-effects at doses well below tolerance. Finally, by co-administration with rAAV2-retro for tracing connections in macaque visual cortex, we found that doxorubicin could also enhance rAAV transduction at remote locations, consistent with retrograde axonal transport from the site of injection. In sum, our findings offer a feasible strategy that can complement vector system optimization for rapid and efficient *in vivo* rAAV transduction in the mammalian CNS.

Results

Doxorubicin enhances rAAV transduction with no impact upon cell tropism

We began by evaluating the effect of doxorubicin in the cerebral cortex of cat, a well-studied mammalian model (Vite et al., 2003). For our standard vector we selected rAAV8, a serotype isolated from rhesus monkey with the express aim of developing a vector for gene therapy with minimal immunogenicity in human tissues (Gao et al., 2002). rAAV8 proved to have a CNS transduction capability superior to that of rAAV2 (Broekman et al., 2006) and could mediate efficient transduction after intraparenchymal injection in various cortical structures of primate brain (Gilkes et al., 2016; Masamizu et al., 2010). rAAV8-hSyn-EGFP, a rAAV8 vector which encoded green fluorescent protein (GFP) under the neuron-specific promoter hSyn, was constructed and infused into cat visual cortex via stereotactic injection at 1×10^9 vector genome (vg) per injection, combined with 10 μg/ml doxorubicin (left hemisphere) or vector alone (right hemisphere)(**Figure 1A**). GFP expression was determined with standard histological techniques thirty days later. As revealed by fluorescence images of brain sections, pressure-injection of vector solution led to focal transduction within a radius of 750 μm, with GFP expression in cell bodies and axons projecting to extrinsic structures (**Figure 1B**). Compared with the control group, GFP fluorescence in doxorubicin-treated group was

noticeably brighter, with intensity significantly increased (~2.5-fold) by doxorubicin (1015 ± 58.4 vs 405.5 ± 46.1, $p < 0.001$; **Figure 1C**). Consistent with studies in mouse and marmoset (Watakabe et al., 2015), rAAV8-mediated GFP expression was not homogeneous across cortical layers, with layer 4 the weakest. As indicated by neuronal-specific marker NeuN, confocal images revealed that the proportion of GFP-expressing neurons was markedly increased, exhibiting higher fluorescence across all cortical layers when treated with doxorubicin (layer 2/3: 92.5 ± 1.5% vs 81.7 ± 2.1%; layer 4: 79.4 ± 2.8% vs 41.3 ± 2.8%; layer 5: 92.2 ± 2.2% vs 78.1 ± 1.7%; layer 6: 91.6 ± 1.6% vs 75.4 ± 2.5%, all $p < 0.01$; **Figure 1D**). Across all layers the average ratio of GFP-positive neurons was 90 ± 2% in the doxorubicin-treated group, compared with 70 ± 2% in the control group (**Figure 1D**). More notably, after a tenfold decrease of vector dose at 1×10^8 vg per injection, doxorubicin treatment still gave an equivalent level of GFP expression to the control at 1×10^9 vg per injection (403.3 ± 32.8 vs 405.5 ± 46.1).

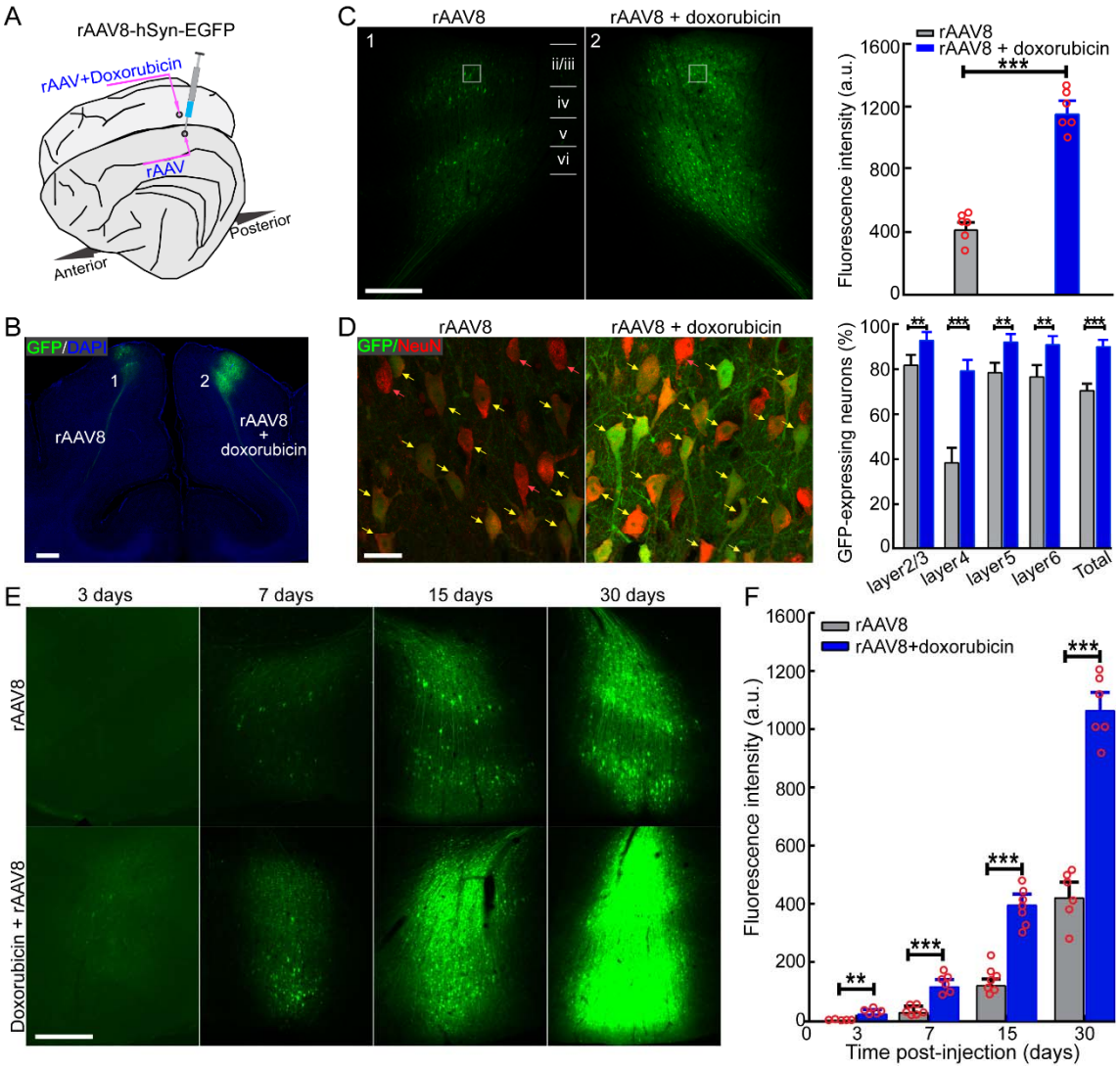

Figure 1. Doxorubicin promotes and accelerates rAAV8-mediated gene transduction in cat visual cortex. (**A**) Schematic representation of injections. rAAV8-hSyn-EGFP alone or coupled with 10 μg/ml doxorubicin were delivered into the left and right hemisphere of cat visual cortex, and GFP fluorescence was examined after 3~30 days of expression. (**B**) Representative image of GFP fluorescence in the control and doxorubicin-treated sites. Blue, DAPI; green, GFP. Scale bar, 1 mm. (**C**) Cortical fluorescence intensity comparison after 30 days of expression. n = 6

injections from 3 cats per group. Unpaired two-tailed t-test; Scale bar, 500 μm. (**D**) Transduction efficiency assessed by colocalization of GFP and NeuN marker. Left: confocal images of GFP expression and NeuN staining of layer 2/3 (boxed in **C**). Yellow arrows, GFP-positive neurons; red arrows, GFP-negative neurons; Scale bar, 25 μm. Right: quantification of transduction efficiency across cortical layers. 5 injections from 3 cats per group; unpaired two-tailed t-test. (**E**) Representative image of GFP expression at the specified time points. The gamma value was adjusted equally to enable the visualization of GFP signals at 3 days. Scale bar, 500 μm. (**F**) Quantification of GFP intensity at varied intervals post-injection. 5-7 injections per group; unpaired two-tailed t-test; data are presented as mean ± SEM. *p <0.05, **p <0.01, ***p <0.001.

To determine whether the effect of doxorubicin on rAAV transduction is exclusive to neurons, we replaced hSyn with an ubiquitous promoter CAG. The modified viral vector, rAAV8-CAG-EGFP was then administered at 5×10^8 vg per injection, vector alone or coupled with 10 μg/ml doxorubicin. The phenotypes of transduced cells were determined by immunohistochemical detection of cell-type-specific markers, i.e. NeuN for neurons, glial fibrillary acidic protein (GFAP) for astrocytes and ionized calcium binding adaptor molecule (Iba-1) for microglia (**Figure 1–figure supplement 1A-C**). As anticipated, we found that under the control of CAG promoter GFP was expressed not only in neurons ($NeuN^+$) but also in astrocytes ($GFAP^+$); fluorescence intensity (NeuN, $p = 0.0061$; GFAP, $p = 0.0068$; **Figure 1–figure supplement 1D**) and the proportions of both GFP-positive neurons and astrocytes were significantly increased in the doxorubicin-treated group relative to the control (neuron: 41 ± 4% vs 21 ± 6%; astrocyte: 32 ± 6% vs 14 ± 4%; all $p < 0.05$, **Figure 1–figure supplement 1E**). With or without doxorubicin, there was no detectable signal in microglia (**Figure 1–figure supplement 1C,E**), consistent with experience to date that this cell class is relatively refractory to transduction by rAAV vector (Maes et al., 2019). These results suggest that doxorubicin treatment enhances neuronal transduction by rAAV8 vector, with no quantitative impact upon its cellular tropism, which is governed by the vector's capsid (Srivastava, 2016).

Doxorubicin accelerates rAAV-mediated gene expression

Practical, rapid onset of rAAV-mediated gene expression is highly significant in regard to studies of brain development, as well as treatment of diseases that require timely intervention (Krol and Feng, 2018). To explore the impact of doxorubicin on the onset of neuronal transduction, we carefully examined the time course of transgene expression in doxorubicin-treated versus control groups. Following our established procedure, rAAV8-hSyn-EGFP alone or coupled with 10 μg/ml doxorubicin was infused into cat visual cortex at 1×10^9 vg per injection, and GFP expressions were determined with standard histological techniques at 3, 7, 15 and 30 days following injection (**Figure 1E**). We found that the pace of transgene expression was greatly accelerated in the presence of doxorubicin. In the control group, GFP fluorescence could be detected no earlier than 7 days post-injection. This reduced to 3 days for the doxorubicin-treated group, with a steady increase in GFP expression

thereafter. At 7 days after injection, GFP activity in the doxorubicin-treated group was about 4-fold higher than that in the control group (104.3 ± 9.6 vs 25.2 ± 2.5), actually matching the 15-day level (104.3 ± 9.6 vs 118.7 ± 10.9)(**Figure 1E**). Throughout the period of examination, GFP expression in doxorubicin-treated group consistently exceeded the control group (3 days: $p = 0.0015$; 7 days: $p = 0.0003$; 15 days: $p < 0.0001$; 30 days: $p < 0.0001$; **Figure 1F**). These results reveal that doxorubicin significantly accelerates rAAV transduction, facilitating timely interventions in the CNS by means of rapid and efficient transgene expression.

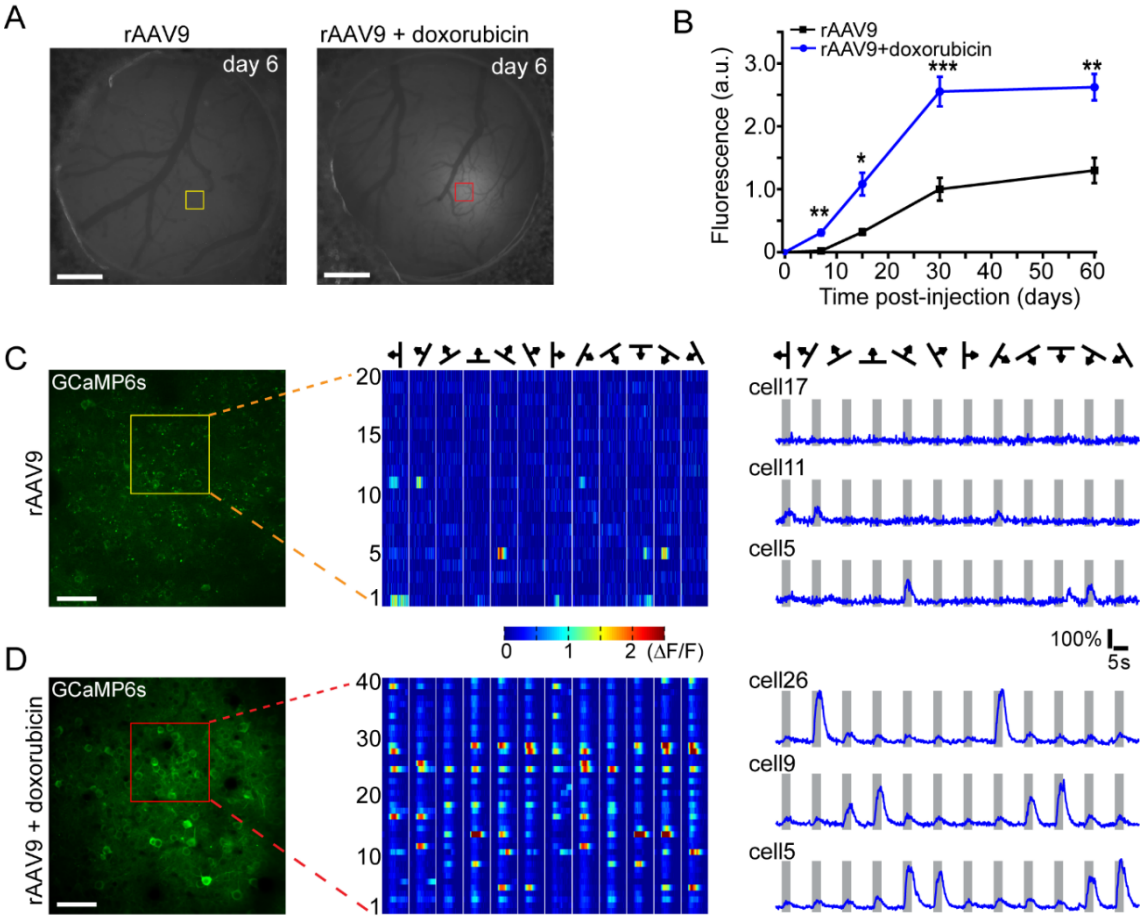

Figure 2. Doxorubicin induces a rapid onset of transgene expression for in vivo imaging of neural function. (**A**) Representative fluorescence images of mouse V1 six days after vector administration (rAAV9-hSyn-GCaMP6s vector: 2×10^{12} vg/ml, 1 μl per injection). Scale bar, 1 mm. (**B**) *In vivo* tracking of GCaMP6s expression following administration in mouse visual cortex. 5 mice per group; unpaired two-tailed t-test, mean ± SEM. *$p < 0.05$. **$p < 0.01$. ***$p < 0.001$. (**C,D**) *In vivo* two-photon image of Ca^{2+} fluorescence assessed after only 6 days of expression at a focal plane of injection sites ~120 μm below cortical surface, as indicated in **A**. Mean fluorescence changes (ΔF/F) of sampled cells (boxed in **C,D**) evoked by drifting sine-wave grating stimuli. Scale bar, 50 μm.

To confirm these findings, we also tracked transgene expression *in vivo* with two-photon imaging in mice. After a delivery of 2×10^{9} vg of rAAV9-hSyn-GCaMP6s into mouse V1, vector alone or combined with 10 μg/ml doxorubicin, the expression of GCaMP6s indicator was monitored with two-photon Ca^{2+} imaging. As shown by **Figure 2** for a large window of brain surface, the fluorescence signal in doxorubicin-treated site was evident at the sixth day following injection, at which time point it was

undetectable in the control site (**Figure 2A**). Doxorubicin treatment more than doubled the rate of expression, reaching a plateau at 30 days under doxorubicin treatment, in comparison to ~50% of this level at around 60 days in the control (6 day, $p = 0.003$; 15 day, $p = 0.0133$; 30 day, $p = 0.0003$; 60 day, $p = 0.0011$; **Figure 2B**). When examined with two-photon microscopy at the sixth day, the morphology of cell bodies was clearly observed under doxorubicin-treated conditions. Accordingly, using drifting sine-wave gratings as visual stimuli, robust direction-selective responses of mouse V1 neurons could be recorded in the doxorubicin-treated areas, but not in the control (**Figure 2C,D**); comparable neural activities in untreated mice could only be obtained until two weeks post-administration. At a comparative expression level of GCaMP6s, e.g. the 15th day of doxorubicin-treated versus the 30th day of control sites following injections (**Figure 2–figure supplement 1A,B**), we found no significant difference between two groups in the response strength (**Figure 2– figure supplement 1C**), with only a slight reduction in the orientation selectivity of V1 neurons (**Figure 2–figure supplement 1D**). Doxorubicin treatment thus resulted in no observable impairment of neural function.

Altogether, these results revealed that doxorubicin significantly accelerates rAAV-mediated gene transduction, enabling earlier commencement of transgene expression for interventions in the mammalian CNS.

Dose-dependency for doxorubicin enhancement of rAAV-mediated gene expression

To determine the optimal dosage of doxorubicin for *in vivo* neurological administration, a trade-off between efficacy for rAAV transduction versus toxicity to neural tissues, rAAV8-hSyn-EGFP vector was infused into cat visual cortices at 1×10^9 vg per injection in combination with varied concentrations of doxorubicin (range 0-100 μg/ml), and GFP expression was examined seven days post-injection. As shown in **Figure 3A**, GFP expression levels were closely tied to doxorubicin concentration, displaying a steady increase over a range of 0.1 to 30 μg/ml. To mitigate doxorubicin concentration loss through diffusion, GFP intensity was measured within a ROI of 500 x 1000 μm at the core of each injection, as indicated in the control (**Figure 3A**). Quantitative analysis confirmed the dose-dependent enhancement of rAAV-mediated GFP expression by doxorubicin, with the maximum obtained at 30 μg/ml (Control vs 1.0 μg/ml, $p = 0.02$; control vs 3.0 μg/ml, $p = 0.008$; control vs 10 μg/ml, $p = 0.002$; control vs 30 μg/ml, $p = 0.0012$; **Figure 3B**). For the topmost doxorubicin dosage of 100 μg/ml, GFP intensity decreased sharply at the core of injection, hence demonstrating notable cytotoxicity.

To further substantiate the differential dose-effect of doxorubicin, we analyzed the status of GFP-expressing neurons with the nuclear marker DAPI and the neuron-specific marker NeuN (**Figure 3C-F**). Confocal images revealed that cell bodies and neurites of infected neurons exhibited intact, normal morphology after doxorubicin treatment at a dosage from 0.1 to 10 μg/ml. At a dose of 30 μg/ml the

neurites of neurons receded, and cell bodies became round with weak or even absent NeuN signals. When doxorubicin concentration reached 100 μg/ml neurons were completely absent from the core of the injection, with glial accumulations in their place. These data further informed the optimal dosage for use of doxorubicin in the CNS, indicating a ceiling concentration of 10 μg/ml, up to which rAAV-mediated gene transduction is notably enhanced by doxorubicin with negligible cytotoxicity to neural tissues.

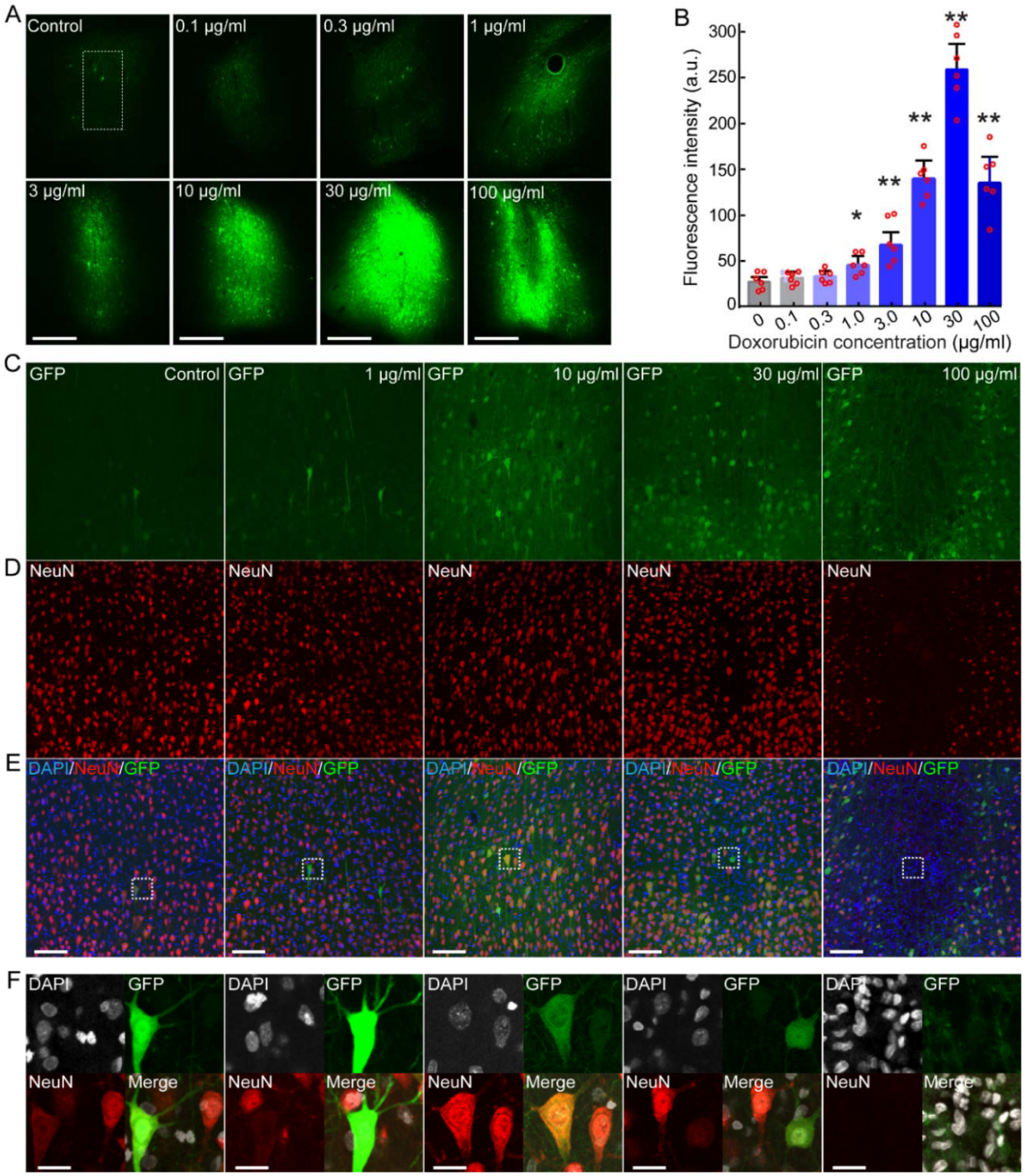

Figure 3. The effect of doxorubicin on rAAV transduction is concentration-dependent, and free from appreciable cytotoxic effects at a dosage from 1 to 10 μg/ml

(**A**) Representative fluorescence images of injections seven days after co-infusion of rAAV8-hSyn-EGFP with varied concentrations of doxorubicin. Scale bar, 500 μm. (**B**) Quantification of core fluorescence intensity (as indicated in the control of **A**). 6 injections from 6 cats per group. One-way ANOVA, post hoc Tukey Kramer correction; mean ± SEM, *$p < 0.05$, **$p < 0.01$. (**C-E**) Status of transduced neurons (GFP, green) at cellular level (**C**), quantified by neural marker NeuN (**D**), and nuclear marker DAPI (**E**). Scale bar, 100 μm. (**F**) Magnified views of neuronal cells under

229 different doxorubicin concentrations (as indicated in the inset of **E**). Scale bar, 20 μm.

230 Locally injected doxorubicin lacks detectable cytotoxicity for neural tissue

231 To establish the safety of *in vivo* neurological administration of doxorubicin at 10 μg/ml, we set out
232 to determine whether or not this concentration has apparent cytotoxic effects upon neural tissues.
233 First, as reported above with two-photon Ca^{2+} imaging, cellular function of neurons was not
234 appreciably affected by doxorubicin (**Figure 2–figure supplement 1**).

235 Next, we used TUNEL assay and immunocytochemistry to assess neuronal apoptosis and
236 inflammatory responses, which are the major contributors to doxorubicin cardiotoxicity and other
237 side-effects (Sauter et al., 2011). Seven days after administration of 10 μg/ml doxorubicin, TUNEL
238 staining was performed and apoptotic cells were screened by confocal fluorescence microscopy. As
239 presented in **Figure 4A**, no appreciable apoptotic effect was observed in either doxorubicin-treated
240 group or the control group, when compared to a positive control treated with DNase I, as indicated
241 by fluorescent-labeled nuclear marker DAPI (**Figure 4A**). In the immunocytochemical study,
242 microglia were detected and counted in brain sections by antibody recognition of its specific marker
243 Iba-1 (**Figure 4B**). Quantitatively, the outcome revealed no difference between the doxorubicin and
244 control groups in regard to the expression of microglia after a single injection (164.0 ± 7.5/mm^2 vs
245 173.2 ± 11.8/mm^2, $p = 0.53$; **Figure 4C**). Co-administration with rAAV8 vector gave a similar result,
246 i.e. the rAAV-plus-doxorubicin group versus the rAAV group (186.2 ± 6.2/mm^2 vs 189.6 ± 5.9/mm^2, p
247 = 0.7; **Figure 4C**), indicating no inflammatory response following a single injection of doxorubicin.

248 Finally, to determine whether doxorubicin treatment might induce any side effects at the
249 behavioral level, we co-infused rAAVs with 10 μg/ml doxorubicin or vector alone (as a control) into
250 the primary motor cortex (M1) of mice and examined locomotor activity fifteen days later. The mice
251 were placed in an open field chamber and allowed 15 minutes for free exploration, monitored by
252 video camera (**Figure 4D**). None of the locomotor parameters analyzed revealed any significant
253 difference in behavior between doxorubicin-treated mice and the control: specifically, total distance
254 traveled (4691 ± 1332 vs 4295 ± 736 cm, $p = 0.28$; **Figure 4E**), mean velocity (5.2 ± 1.5 vs 4.8 ± 0.8cm/s,
255 $p = 0.28$, **Figure 4F**) and time in movement (8.28 ± 0.37 vs 7.77 ± 0.38 min, $p = 0.34$; **Figure 4G**) were
256 all equivalent. Taken together, these data show that local injection of doxorubicin lacks detectable
257 adverse effects upon neural tissue under typical experimental conditions.

258 Doxorubicin enhances rAAV transduction irrespective of rAAV serotype and animal species

259 AAV has multiple serotypes and new variants are continually being developed for experimental and
260 clinical purposes (Wang et al., 2019). To investigate how far our findings represent a general agonist
261 effect of doxorubicin upon rAAV transduction, we employed two other rAAV serotypes: rAAV2 and
262 rAAV-PHP.eB, the latter a variant of AAV9 evoluted to maximize CNS transduction via intravenous
263 administration (Chan et al., 2017). Combined with 10 μg/ml doxorubicin, viral vectors of rAAV2,

rAAV8 and rAAV-PHP.eB encoding GFP under the CAG promoter were injected into cat cerebral cortex and GFP expression was assessed seven days later. We observed similar levels of GFP expression in the control groups of rAAV8 and rAAV-PHP.eB, each significantly better than that achieved by rAAV2 (**Figure 5A**). More importantly, GFP intensity (rAAV2, p = 0.006; rAAV8, p = 0.0094; rAAV-PHP.eB, p = 0.012; **Figure 5B**) and percentage of transduced cells (rAAV2: 15 ± 1% vs 5 ± 1%, p = 0.0086; rAAV8: 37 ± 4% vs 16 ± 1%, p = 0.0094; rAAV-PHP.eB: 35 ± 3% vs 13 ± 1%, p = 0.0005; **Figure 5C**) were both significantly upregulated by doxorubicin in all three serotypes of rAAV, suggesting doxorubicin indeed has a general agonist effect upon gene transduction mediated by rAAV vectors, irrespective of vector serotypes.

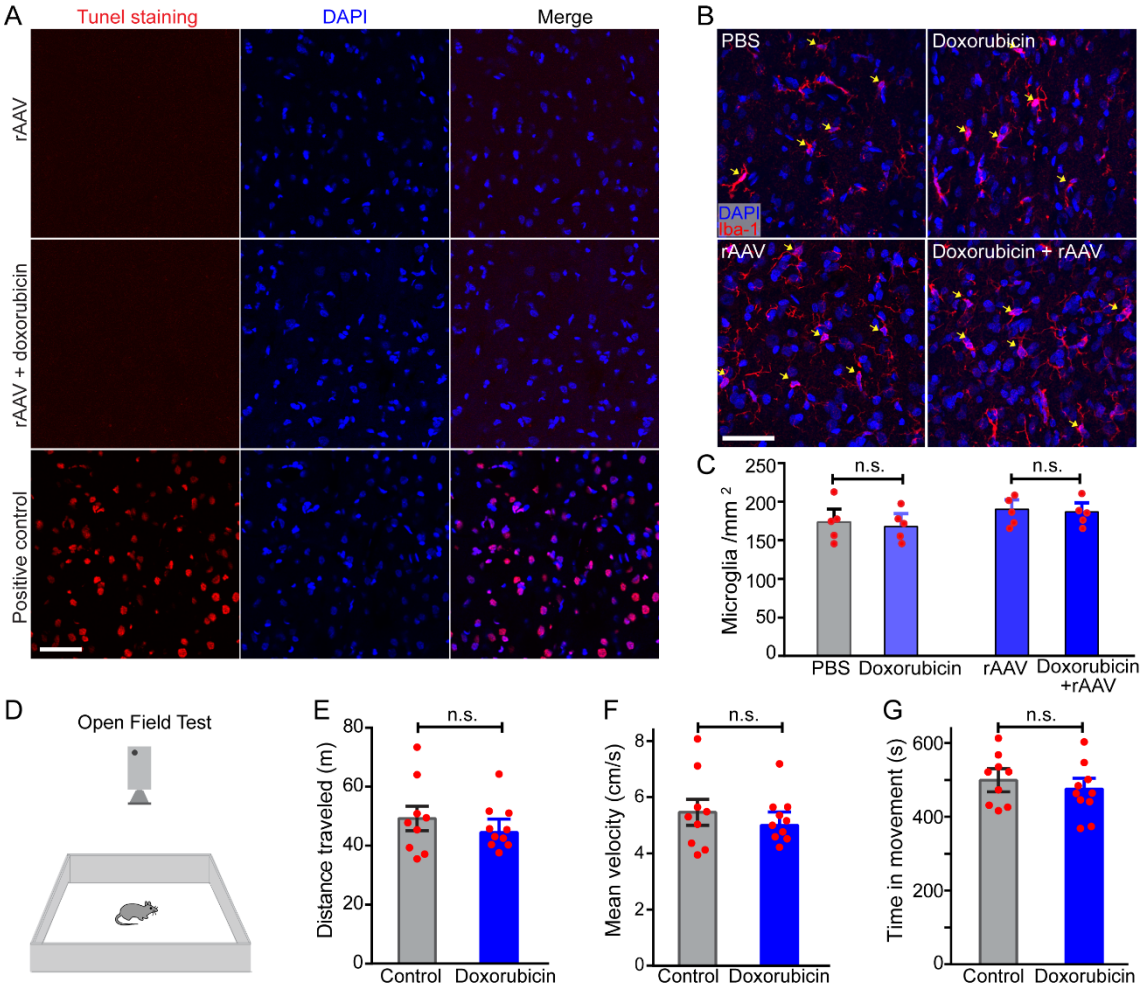

Figure 4. Doxorubicin induces little appreciable side effects on neural tissue under experimental conditions. (**A**) Confocal images of TUNEL stained sections seven days after administration of rAAV8 alone or with doxorubicin. Positive control samples pretreated with DNase I. Blue, DAPI; red, apoptotic cell. Scale bar, 50 μm. (**B**) Representative images of fluorescent-labeled microglia cells (yellow arrows) by immunohistochemical detection of Iba-1; blue: DAPI, red: Iba-1. Scale bar, 50 μm. (**C**) Quantification of microglia cell numbers in the test sites. 5 injections per group. Unpaired two-tailed t-test; mean ± SEM. (**D**) Schematic diagram of open field test. rAAV8-hSyn-EGFP vector was administered into mouse M1 with or without doxorubicin, and mice were placed in an open field chamber (40 x 40 cm) to allow 15 minutes for free exploration 15 days post-injection. (**E-G**) Quantification of distance traveled (4691 ± 1332cm vs 4295 ± 736cm, p = 0.28, Wilcoxon rank-sum test), mean velocity (5.2 ± 1.5 vs 4.8 ± 0.8cm/s, p = 0.28, Wilcoxon rank-sum test) and time in movement (8.28 ± 0.37min vs 7.77 ± 0.38min, p = 0.34, Unpaired two-tailed t-

test) between doxorubicin-treated mice and the control. For quantification: n = 9 and n =10 mice in the control and doxorubicin groups, mean ± SEM

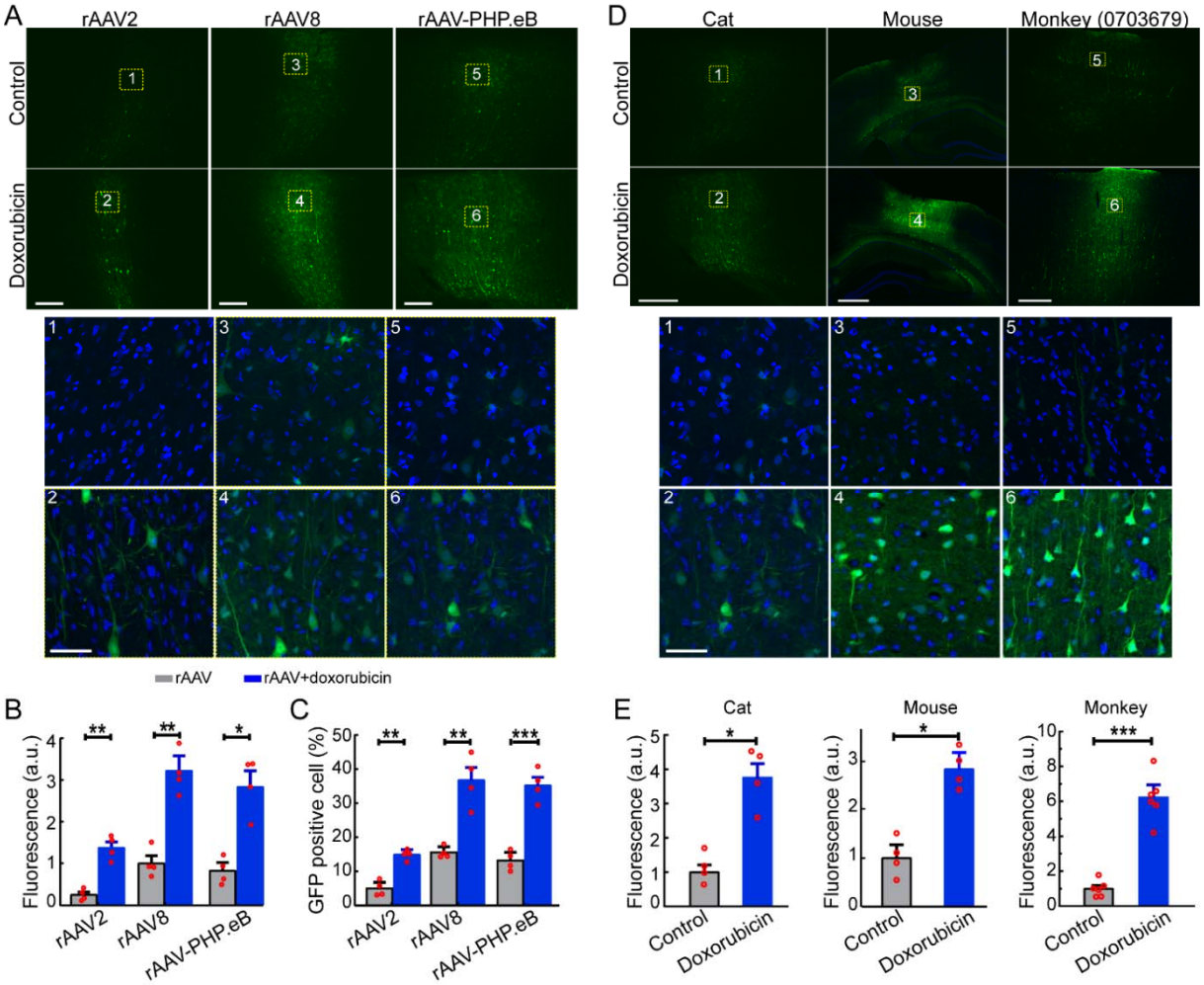

Figure 5. The agonist effect of doxorubicin is reproducible with different rAAV serotypes and animal species (**A**) Representative images showing GFP expression via viral vectors of rAAV2, rAAV8 and rAAV-PHP.eB under the CAG promoter. Upper panel: images of the injection sites pertaining to rAAV2, rAAV8 and rAAV-PHP.eB vector, respectively. Scale bar, 250 μm. Lower panel: magnified views of the boxed regions 1-6. DAPI: blue, GFP: green. Scale bar, 50 μm. (**B,C**) Quantification of mean GFP intensity and percentage of transduced cell. 4 injections from 4 cats per group; unpaired two-tailed t-test. (**D**) Representative images of vector injection-sites from the cerebral cortex of cat, mouse and macaque monkey. rAAV-PHP.eB-CAG-EGFP vector was used and GFP expression was assessed after seven days of expression. Lower panel: magnified views of the boxed regions 1-6. DAPI: blue, GFP: green. Scale bar, 500 μm (upper), 50 μm (lower). (**E**) Quantification of mean GFP intensity in cat, mouse and monkey. For quantification, 4 injections from 4 animals per group in cat and mice, and 6 injections per group from two monkeys; unpaired two-tailed t-test; mean ± SEM, *p <0.05,**p <0.01. ***p <0.001.

We further tested the effect of doxorubicin in the cerebral cortex of different animal species. After an infusion of rAAV-PHP.eB-CAG-EGFP into the cerebral cortex of mouse, cat and macaque monkey (**Figure D**), we obtained a substantial, quantifiable enhancement of transgene expression across all three mammalian species under doxorubicin treatment (Cat, p = 0.012; Mouse, p = 0.011; Monkey, p = 0.0006; **Figure 5E**). Qualitative examples of the enhancement of doxorubicin in macaque

motor cortex were further shown in **Figure 5–figure supplement 1**. These results indicated that doxorubicin may well exert a general effect upon rAAV transduction, regardless of rAAV serotypes and host species.

Doxorubicin enables efficient retrograde tracing of connections in macaque cortex and thalamus

Finally, motivated by previous reports that doxorubicin undergoes retrograde transport from uptake at axonal terminals (Bigotte and Olsson, 1982; Koda and Van der Kooy, 1983), we considered that doxorubicin have good prospects for remote circuit-selective enhancement of rAAV transduction and therefore could be used for neural circuit interrogation. For this aim we coupled doxorubicin with rAAV2-retro, a vector recently developed for the express purpose of maximizing retrograde access to projection neurons (Tervo et al., 2016).

We conducted this experiment in rhesus monkey by infusing rAAV2-retro-CAG-tdTomato bilaterally into area V1, either with 10 μg/ml doxorubicin (right hemisphere) or vector alone as a control (left hemisphere) (**Figure 6A**). Six weeks after injection, we examined tdTomato expression amongst retrogradely labeled cells in the lateral geniculate nucleus (LGN), as well as cortical areas including V2, V4 and V5/MT that send long-range projections to V1. Before examination, we first confirmed good rAAV2-retro transduction across cortical layers at the injection site of V1 (**Figure 6B**). In the LGN, the principal subcortical source of input to V1, we observed dense clusters of neurons labeled with tdTomato (**Figure 6C**). Consistent with previous reports based on tracer dyes (Angelucci and Sainsbury, 2006; Kennedy and Bullier, 1985), the cell bodies of these neurons were concentrated in a narrow strip across the six-layer structure, surrounded by nerve fibers. Compared with the control side, the number of cells labeled with tdTomato on the right side of LGN was far greater, and tdTomato expression was much stronger in both neuron cell bodies and fibers (**Figure 6C**,**D** and **Figure 6–figure supplement 1A**). Amongst prestriate cortical areas, we found large numbers of tdTomato-labeled cells in V2, concentrated in a retinotopically matching subregion close to the injection site in V1 (**Figure 6E**), consistent with previous studies (Perkel et al., 1986; Weller and Kaas, 1983). Compared with the left control side, the number of tdTomato-positive cells in the right V2 was greater, and the fluorescent signal was stronger across serial sections (**Figure 6F** and **Figure 6–figure supplement 1B**), confirming the enhancement effect of doxorubicin to be mediated via retrograde transport in corticocortical as well as thalamocortical projections. This enhancement became more clear in weak or moderate long-range projections – we detected numerous tdTomato-positive neurons in V4, V5/MT and other visual cortices in the right hemisphere, with little or no corresponding tdTomato signal in the left control side; in this respect, performance of rAAV2-retro unaided by doxorubicin was notably poor in comparison to conventional retrograde tracers (**Figure 6G-I** and **Figure 6–figure supplement 1C,D**). These results indicated that doxorubicin can induce remote enhancement of rAAV transduction via axonal retrograde transport in both thalamocortical

and corticocortical projections, and could thus be a useful tool for analysis of neural circuits in large mammals like the macaque.

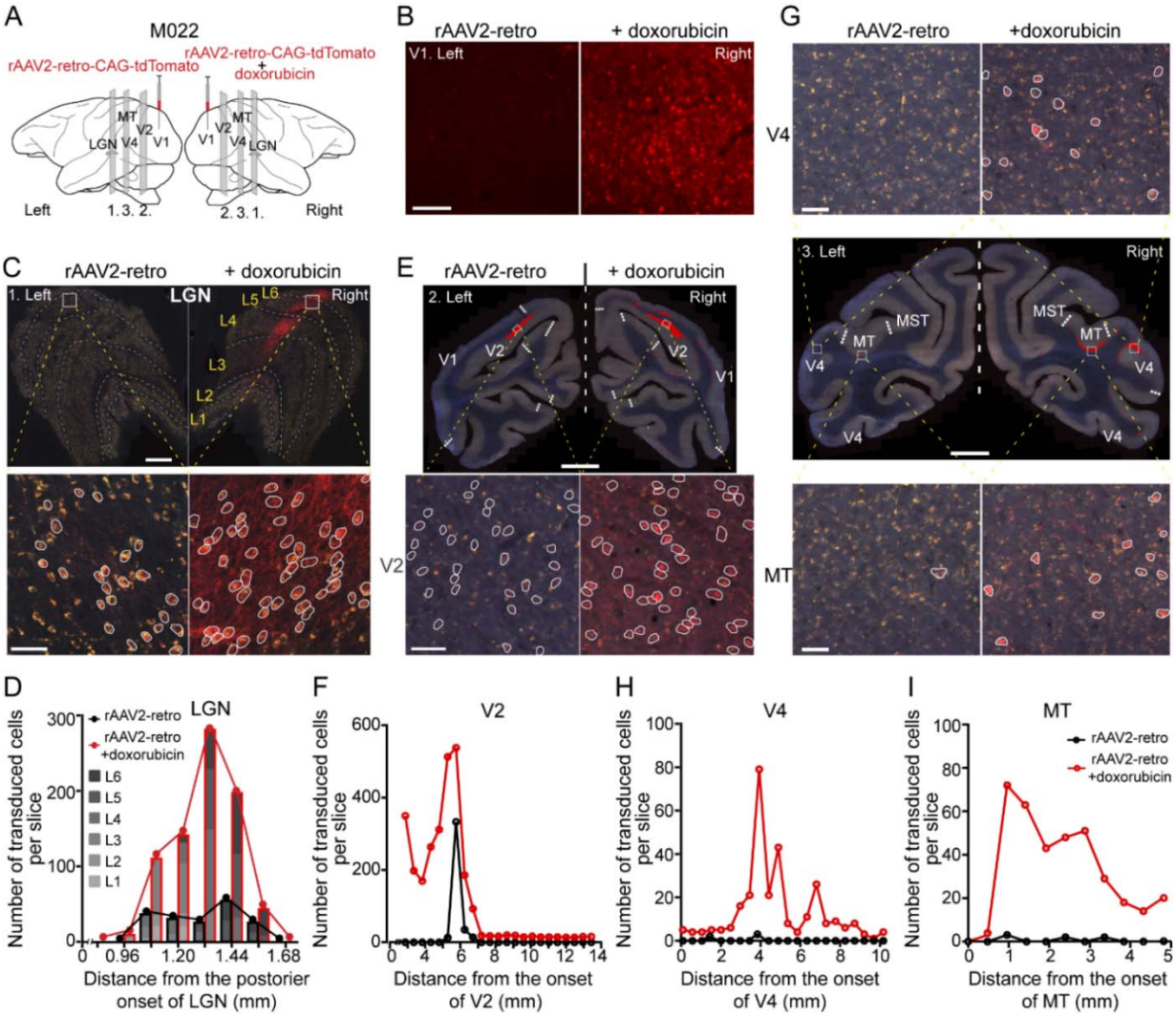

Figure 6. Enhancement of rAAV transduction via retrograde axonal transport in macaque thalamo- and cortico-cortical circuits

(**A**) Schematic showing injections and quantified sources of afferents to V1, including LGN (panel 1), V2 (panel 2), V4 and MT (panel 3). rAAV2-retro-CAG-tdTomato, vector alone or coupled with doxorubicin was infused at symmetrical locations in the left and right hemisphere of monkey V1. Transduced neurons were assessed six weeks later. (**B**) Representative images of neuronal transduction at the injection site. Scale bar, 100 μm. (**C**) Representative images of neuronal transduction in LGN. Transduced neurons from ROI (boxed in the upper panel) were marked by white circles. Scale bar, 500 μm (upper), 50 μm (lower). (**D**) Comparison of retrograde transport efficiency for LGN. Transduced cells were counted in sample sections taken every 120 μm across LGN. (**E**) Representative images of neuronal transduction in V2. Upper panel: whole coronal image (transduced cells are marked with red dots); Lower panel: transduced neurons from ROI (boxed in the upper panel) are marked by white circles. Scale bar, 5000 μm (upper), 50 μm (lower). (**F**) Comparison of retrograde transport efficiency for V2. (**G**) Representative images of neuronal transduction in V4 and MT. Middle panel: whole coronal image of macaque brain (transduced cells are marked with red dots); Top and bottom panels: transduced neurons from ROIs of V4 and MT are marked by white circles. Scale bar, 5000 μm (middle), 50 μm (top and bottom). (**H-I**) Comparison of retrograde transport efficiency for V4 and MT. In **F**,**H** and **I,** transduced cells were counted in regions of V2, V4 and MT within sample sections taken every 480 μm across the brain from posterior to anterior.

359 ## *Discussion*

360 With recent advances in vector engineering, rAAVs have met with great success as carriers for *in vivo*
361 gene transfer. Clinical trials of rAAV-based gene therapy have demonstrated clear therapeutic efficacy
362 (Manno et al., 2006; Mendell et al., 2017). rAAV has also become a powerful tool for cell type-specific
363 gene modulation in many fields of basic neuroscience (Betley and Sternson, 2011). However, it is also
364 recognized that rAAV still has some shortfalls, which include insufficient transduction and tardiness
365 of gene expression in targeted tissues (Wang et al., 2019). Therefore, more efficient strategies for
366 rapid-onset and high-level transgene expression at lower doses are much desired for *in vivo* rAAV
367 transduction. Here we outline how the clinical pharmacological agent ***doxorubicin*** might be
368 exploited to enhance the efficiency of transgene expression in a range of basic and therapeutic
369 research applications across various combinations of rAAV serotype and experimental species.

370 ### Mechanism and time course of doxorubicin action

371 After infection of the host cell the genome of rAAV has to undergo several processes before transgene
372 expression can occur, amongst which intracellular trafficking and second-strand DNA synthesis are
373 two rate-limiting steps (Ferrari et al., 1996; Harbison et al., 2008). The action of doxorubicin – an
374 inhibitor of topoisomerase II and DNA synthesis (Tacar et al., 2013) – to facilitate this process is
375 therefore paradoxical. A clue may exist in the long-known finding that agents causing DNA damage,
376 including ionizing radiation, have the same general capability as topoisomerase-inhibitors to enhance
377 the efficiency of rAAV transduction (Alexander et al., 1994; Kanazawa et al., 2001; Nicolson et al., 2016;
378 Russell et al., 1995). This capability may, perhaps, be an indirect consequence of the cellular reaction
379 to DNA damage: the 'decoy' thesis posits that rAAV replication is normally restrained by DNA-damage
380 response proteins, which become preferentially engaged in the work of DNA repair (Choi et al., 2006;
381 Nicolson et al., 2016). Furthermore, doxorubicin may also promote viral nuclear entry through
382 modulation of proteasome function (Yan et al., 2004). We embarked on a series of experiments testing
383 the effect of doxorubicin upon transgene expression mediated by rAAV8 in cat cortex, and observed
384 a remarkable enhancement of transduction following doxorubicin treatment (**Figure 1**), consistent
385 with previous studies utilizing rAAV2 (Zhang et al., 2012; Zhang et al., 2009). Furthermore,
386 doxorubicin enhanced the rapidity of cellular transduction by rAAV: we found that the time required
387 for transgene expression to reach detection level decreased from around 7 days to 3 days, with a
388 sustained increase of expression thereafter (**Figure 1F** and **2**). In short, we infer doxorubicin to have
389 an intracellular action that favors the accrual of stable, dual-stranded AAV DNA as an 'episome' within
390 the cell nucleus. This augments expression of the viral DNA, subject to any regulatory elements
391 included within the vector genome. Subsequent investigation served to confirm the generality of this
392 accelerated transduction achievable with doxorubicin.

The generality of doxorubicin-mediated transduction enhancement

AAV has multiple serotypes with varying characteristics and new AAV variants with superior efficacy continue to be developed through vector engineering approaches, that essentially seek to 'fine-tune' the binding properties of the capsid to cell surface receptors (Wang et al., 2019). To examine the plurality of doxorubicin enhancement we extended our study of rAAV8 to other AAV serotypes such as rAAV2, rAAV9 and rAAV-PhP.eB, and found that all three showed comparable, marked enhancement by doxorubicin, suggesting a serotype-general effect of doxorubicin upon rAAV transduction. For further substantiation, we extended our investigation across species, and found that doxorubicin achieved similar levels of enhancement for transduction by rAAV-PhP.eB in the cortex of macaque monkey and mouse, as it did in the cat (**Figure 5D**,**E**).

In addition to species- and serotype-generality, we also assessed whether doxorubicin perturbs the specificity of transgene expression across different cell types, either by interfering with the cell tropism of rAAV vector, or with the cell-specific regulation of transcription. Our experiments allowed us to compare the action of doxorubicin in conjunction with rAAV vectors carrying either the neuron-specific hSyn or the ubiquitous CAG promoter. Consistent with previous studies (Watakabe et al., 2015), we found a proclivity for transduction that cortical layer 4, characterized by smaller pyramids, showed minimal transduction with rAAV8 under the neuron-specific promoter (hSyn) and the greatest proportional increase with doxorubicin. Most importantly, with hSyn promoter, transgene expression with doxorubicin remained restricted to neurons (**Figure 1D**), giving no evidence of doxorubicin interference with the cell-type specificity governed by promoters. With CAG promoter we observed additional expression of transgene by astrocytes; doxorubicin treatment induced a similar enhancement in both neurons and astrocytes, but did not alter the negative status of microglia transduction (**Figure 1–figure supplement 1**). We therefore obtained no indication that doxorubicin can alter the fundamental tropism of rAAV vectors.

Given what is known of the molecular biology of doxorubicin action (reviewed above), the ensemble of our findings suggests the analogy to chemical catalysis: doxorubicin enhances the speed and level of transgene expression, but does not affect the tropism for cell type (as governed by the capsid), nor alter the specificity of cellular expression (as governed by regulators of transcription). Hence, in principle, doxorubicin enhancement should prove a valuable strategy for optimizing rAAV transduction in many fields of research practice.

Absence of neurotoxicity at an effective clinical dosage

Cytotoxicity is the foremost concern prohibiting exogenous agents from *in vivo* application (Nicolson et al., 2016; Russell et al., 1995; Yan et al., 2004). As a chemotherapeutic drug, doxorubicin takes effect in cancer treatment by inhibiting cell proliferation and inducing apoptosis (Tacar et al., 2013). For non-dividing cells, there is less expectation of significant cytotoxicity. Direct delivery into the brain, rather

than intravenous administration, restricts doxorubicin uptake to cells within local injection area. Our *in vivo* dose-finding study found that doxorubicin significantly enhances rAAV transduction at a concentration of 1~10 μg/ml (or 1.72~17.2 μM) (**Figure 3**). At a concentration of 10 μg/ml, we detected little cytotoxicity: infected neurons maintained healthy morphology and function upon histological examination (**Figure 1D** and **3**) and *in vivo* imaging (**Figure 2** and **Figure 2–figure supplement 1**) at 7~30 days post-injection. Further examinations revealed no apoptosis at the site of injection (**Figure 4A**), nor any inflammatory response (**Figure 4B**). At the behavioral level, our trial animals (mice) also presented normal locomotor activity (**Figure 4E-F**). This non-neurotoxic concentration of doxorubicin (1.72~17.2 μM) is within the 10-24 μM range of peak bloodstream plasma concentrations following doxorubicin administration (50 mg/m^2) in clinical cancer chemotherapy (Mross et al., 1988). Furthermore, following direct injections into the cortex, or other brain sites, the concentration will fall several-fold upon diffusion through neural tissues. Overall, these results confirm the feasibility of the use of doxorubicin to catalyze rAAV transduction at a dosage effectively matching clinical practice.

How could doxorubicin-enhanced transduction work in practice?

Our approach mimics many research applications in seeking to transduce neurons at restricted cortical loci (Scanziani and Hausser, 2009). This includes induction of GCaMP6 for two-photon imaging of neural activity, or a marker like GFP to reveal efferent axon terminals, or an effector such as ChR2 to allow optical modulation of neural activity. The demonstration of remote enhancement via retrograde transport upon rAAV2-retro, further expands potential doxorubicin applications to neural circuit interrogation (Tervo et al., 2016). More importantly, when extended for applications that seek to transduce extensive cortical regions or subcortical nuclei of large volume (e.g., putamen) with convection-enhanced delivery (CED) technique (Mehta et al., 2017), here co-infusion of rAAV vector and doxorubicin could make a strategic difference to the practicality and outcome of both research and therapeutic projects, raising the ceiling for what is considered feasible. Finally, systemic delivery via intravenous injection is generally applied for broad gene delivery to the nervous system (Foust et al., 2009), and this route provides good safety and convenience, especially for clinical purposes. rAAV9 and several other AAV variants, including one that we tested in macaques (rAAV-PHP.eB) have been derived specifically for this route to achieve broad neural transduction within mammalian CNS (Chan et al., 2017; Dayton et al., 2012). However, this route requires substantially high vector load, and faces the challenge of natural immunity (Mingozzi et al., 2007). The enhancement effect of doxorubicin upon transduction would provide great advantages. Combined with BBB opening techniques such as hyperosmotic mannitol or focused ultrasound (Alli et al., 2018; Fu and McCarty, 2016), doxorubicin might prove to be of great avail for rAAV-based gene therapy of neurological diseases. Intravenous co-administration might be applied to address acute conditions such as stroke, exploiting the speedier transgenic expression achievable with doxorubicin. Past gene

463 therapy studies for animal models of stroke have demonstrated benefits from a variety of transgenes,
464 typically administered by direct injection of rAAV, but *prior* to the experimental induction of ischemia
465 (Craig and Housley, 2016; Lu et al., 2012). The effective doubling of the rate of transduction achievable
466 with doxorubicin could provide the key to unlock the clinical potential of transgenic therapy in such
467 emergency contingencies.

468 In summary, our study has demonstrated that application of doxorubicin facilitates rAAV
469 transduction in rodent, carnivore and primate cerebral cortex. This enhancement of doxorubicin
470 takes effect at doses well below tolerance without detectable cytotoxicity to neural tissues. Our
471 findings suggest a feasible strategy synergistic with ongoing vector system engineering to optimize
472 rAAV transduction, so to attain more rapid and more efficient transgene expression *in vivo*.
473

474 # Materials and Methods

475 ## Key resources table

REAGANT or RESOURCE	SOURCE	IDENTIFIER
Bacterial and Virus Strains		
rAAV8-hSyn-EGFP	ION Gene Editing Core Facility	N/A
rAAV8-CAG-EGFP	ION Gene Editing Core Facility	N/A
rAAV-PHP.eB-CAG-EGFP	ION Gene Editing Core Facility	N/A
rAAV2-CAG-EGFP	Taitool Bioscience (Shanghai)	N/A
rAAV9-hSyn-GCaMP6s	Taitool Bioscience (Shanghai)	Cat# S0528
rAAV2-retro-CAG-tdTomato	Got from Dr. Yuejun Chen' Lab	N/A
Chemicals, Peptides, and Recombinant Proteins		
Doxorubicin hydrochloride	Sigma-Aldrich	Cat# D1515-10mg
Antibodies		
Mouse anti-NeuN	Millipore	Cat# MAB377; RRID:AB_2298772
Rabbit anti-GFAP	Invitrogen	Cat# MA119170; RRID:AB_1074604
Rabbit anti-Iba1	Wako	Cat# 01919741; RRID:AB_839504
goat anti-mouse antibody, Alexa Fluor 555	Life Technologies	Cat# A21424; RRID:AB_141780
goat anti-rabbit antibody, Alexa Fluor 555	Life Technologies	Cat# A32732; RRID:AB_2633281
Critical Commercial Assays		
One Step TUNEL Apoptosis Assay Kit	Beyotime technology	Cat# C1089
Experimental Models: Organisms/Strains		
Mouse: C57BL/6	SLAC laboratory	N/A
Cat	ION animal facility	N/A
Rhesus Macaque (Macaca mulatta)	ION Primate Center, Shanghai	N/A
Software and Algorithms		
ImageJ	NIH	RRID:SCR_003070
GraphPad Prism 7	GraphPad	RRID:SCR_002798
MATLAB	MathWorks	RRID:SCR_001622
Other		
E80i microscopy	Nikon	N/A

VS120 virtual slide microscope	Olympus	N/A
TiE-A1plus Laser Scanning Confocal microscope	Nikon	N/A
Axio Scan Z1 fluorescence microscope	ZEISS	N/A
Two-photon microscope	Thorlabs	N/A
Axio Scan. Z1	ZEISS	N/A
Ti-Sa laser	Spectra-physics	N/A

Animals

All experimental procedures were approved by the Animal Care and Use Committee of the Institute of Neuroscience, Chinese Academy of Sciences. Experimental subjects contained adult cats, C57BL/6 mice and rhesus macaques (Macaca mulatta). Thirty adult cats of both sexes (age: 1-3 years; weight: 2.5-3.5 kg) were obtained through the animal facility of the Institute of Neuroscience. Thirty-three Male C57BL/6 mice of 8 weeks age were purchased from Slac Laboratory Animals (Shanghai). Three macaque monkeys (two males and one female, 6-8 years old, weight: 6.0-9.0 kg) were used in this study, two for cross-species examination and another for neural circuit interrogation. All animals were raised under constant temperature, humidity and automatic light cycles.

Virus and drug preparation

The rAAV vectors and sources were the following: rAAV8-hSyn-EGFP, rAAV8-CAG-EGFP, rAAV-PHP.eB-CAG-EGFP (ION Gene Editing Core Facility), rAAV2-CAG-EGFP, rAAV9-hSyn-GCaMP6s (Taitool Bioscience, Shanghai) and rAAV2-retro-CAG-tdTomato (obtained from Dr. Yuejun Chen' Lab). Doxorubicin (doxorubicin hydrochloride, Sigma-Aldrich) was dissolved in sterile phosphate buffered saline (PBS) and stored at -80°C. For injection, viral solutions were diluted and prepared with PBS just before experiment, which consisted of rAAV and 10 μg/ml doxorubicin (or as indicated). As a control, viral solutions contained only rAAV vector in PBS.

Surgery and stereotaxic injection

For virus injection, adult cats were anaesthetized with ketamine hydrochloride (25 mg/kg) and then positioned in a custom-made stereotaxic apparatus with anesthesia maintained by isoflurane (1.5-2.0%). Small skull holes (~1 mm^2) were made in both hemispheres at Horsley-Clarke coordinates A5-P7, L2-L3. Dura incisions were made for introduction of glass pipettes (tip diameter of 40-50 μm) into the cerebral cortex (at a depth of ~1000 μm from cortical surface). Injections of viral solutions were performed through glass micropipettes at a rate of 90 nL/min by a microinjector (QSI). After injection, micropipettes were kept in place for 10 minutes prior to withdrawal. Pulse oxygen saturation, electrocardiograph, end-tidal carbon dioxide and core body temperature were monitored throughout the surgical procedure. After surgery, animals recovered from the anesthetic and cefotaxime sodium (80 mg/kg) was applied through intraperitoneal injection twice a day in the following seven days.

To examine the effect of doxorubicin on rAAV-mediated neuronal transduction, rAAV8-hSyn-EGFP vector (titer: 1×10^{12} vg/ml) was injected into the right and left hemisphere of three cats with or without doxorubicin (10 μg/ml) at a volume of 1000 nl for each injection, respectively. Histological examination was carried out at 30 days post-injection.

To assess the impact of doxorubicin on the kinetics of rAAV transduction, rAAV8-hSyn-EGFP vector (titer: 1×10^{12} vg/ml) coupled with doxorubicin (10 μg/ml) or vector alone was administered into the visual cortex of twelve cats at a volume of 1000 nl for each injection, three cats per group. Histological examination was carried out at 3, 7, 15 and 30 days post-injection.

To define the optimal dosage of doxorubicin for neural administration, different concentrations of doxorubicin (0.1-100 μg/ml) were injected with rAAV8-hSyn-EGFP (titer: 1×10^{12} vg/ml) into the visual cortex of six cats at a volume of 1000 nl for each injection, with injections of vector only as control. Histological examination was carried out at 7 days post-injection.

To assess the cytotoxic effects of doxorubicin upon neural tissues, five cats were injected with PBS, doxorubicin (10 μg/ml), and rAAV8 vector (rAAV8-hSyn/CAG-EGFP, titer: $0.5 \sim 1 \times 10^{12}$ vg/ml) with or without 10 μg/ml doxorubicin at a volume of 1000 nl for each injection. Seven days following injection, animals were prepared for TUNEL assay and inflammatory examination.

To determine whether doxorubicin exerts a general agonist effect upon rAAV transduction, rAAV-CAG-EGFP vectors (rAAV8, rAAV-PHP.eB and rAAV2, titer: 5×10^{11} vg/ml) were injected into the visual cortex of five cats with or without doxorubicin (10 μg/ml) at a volume of 1000 nl for each injection. Histological examination was carried out at 7 days post-injection.

For virus injection in mouse, animals were anaesthetized by 1.5~2.0% isoflurane or intraperitoneal injection of pentobarbital sodium (~40 mg/kg) and mounted in a stereotaxic apparatus with body temperature kept at 37 °C. In the cross-species examination, rAAV-PHP.eB-CAG-EGFP vector (titer: 5×10^{11} vg/ml, 1μl) alone or coupled with 10 μg/ml doxorubicin was injected into the primary visual cortex (V1) of four mice (stereotaxic coordinates: 3.1 mm posterior to bregma, 2.5 mm lateral to midline, 0.6 mm vertical from cortical surface) through a skull hole at a rate of 90 nl/min with a glass pipette (tip diameter of 20 - 30 μm). In the open field test, rAAV8-hSyn-EGFP (titer: 1×10^{12} vg/ml, 1μl) alone or coupled with 10 μg/ml doxorubicin was injected into the primary motor cortex (M1) of the right hemisphere of nineteen mice (stereotaxic coordinates: 0.5 mm anterior from bregma, 1.5 mm lateral from the midline, 0.6 mm vertical from cortical surface). For two-photon calcium imaging, a circular craniotomy (~3 mm diameter) was made to expose the primary visual cortex. rAAV9-hSyn-GCaMP6s (2×10^{12} vg/ml, 1μl) coupled with doxorubicin (10 μg/ml) or vector alone was injected into area V1 of ten mice, at a depth of 0.6 mm beneath the cortical surface. After injection, the dura was removed and a chronic window was made with a custom-made double-layered coverslip covering the cortex. For repeated imaging, a custom-made titanium headplate was implanted with dental acrylic. After surgery, antibiotics were administered by intramuscular injection and animals were given about 7 days (or as indicated) for recovery before experiment.

The three adult macaque monkeys used in this study underwent a similar preparatory procedure. Following induction by ketamine hydrochloride (15 mg/kg), deep anesthesia was maintained with isoflurane (1.5-2.0%) whilst the head of animal was mounted in the stereotaxic apparatus and prepared for craniotomy, durotomy and viral injection. In the cross-species examination, rAAV-PHP.eB-CAG-EGFP vectors (titer: 1×10^{12} vg/ml) were injected into the primary motor cortex (at a depth of 1500 μm) through glass pipettes (tip diameter of 40-60 μm) with or without doxorubicin (10 μg/ml) at a volume of 2000 nL for each injection. For neural circuit interrogation, rAAV2-retro-CAG-tdTomato (titer: 4×10^{13} vg/ml, 1μl per injection) was injected into the left and right hemisphere of monkey V1 symmetrically, vector alone or coupled with doxorubicin (10 μg/ml). Throughout the surgical procedure, pulse oxygen saturation, electrocardiograph, end-tidal carbon dioxide and core body temperature (37~38 °C) were monitored. After injection, micropipettes were kept in place for 10 minutes prior to withdrawal and animals were carefully maintained for recovery. Histological examination was carried out at 7 or 42 days post-injection into M1, and V1, respectively.

Tissue preparation, histology and image acquisition

Animals were deeply anaesthetized with sodium pentobarbital, followed by transcardial perfusion of 0.9% NaCl and 4% paraformaldehyde (wt/vol) in PBS. Brains were removed and post-fixed with 4% paraformaldehyde in PBS for 12 ~ 48 hours, and then dehydrated with 30% sucrose (wt/vol) for about 1 ~ 5 days. For each brain every injection site was identified and marked under a fluorescence stereoscope (Stereo Discovery V20, Zeiss). Fixed brains were cut into 50-μm-thick coronal sections on a freezing microtome. Representative sections from each injection site showing the largest amount of fluorescence were identified and selected for subsequent assay. For immunohistochemistry, sections were first rehydrated with PBS and preincubated with blocking solution (PBS with 1% bovine serum albumin and 0.3% Triton X-100) before incubation with primary antibodies at 4°C overnight. Antibodies against neuronal or glial marker proteins were used as follows: neuron-specific nuclear protein (mouse anti-NeuN, 1:500; Millipore, MAB377), glial fibrillary acidic protein (rabbit anti-GFAP,1:500; Invitrogen, MA119170) and ionized calcium binding adaptor molecule (rabbit anti-Iba1, 1:500; Wako, 01919741). After rinsing with PBS, sections were incubated with secondary antibody (goat anti-mouse antibody, 1:1000, Life technologies, A21424; goat anti-rabbit antibody, 1:1000, Life technologies, A32732) for 2 hours at room temperature. DAPI was added to a final concentration of 1 μg/ml for staining cell nuclei.

Large field images of representative sections from each injection were first examined with Nikon E80i or Olympus VS120 fluorescence microscope using a 10x objective. Confocal fluorescence images were then acquired by Nikon TiE-A1plus confocal laser scanning microscope using a 20x/0.75NA objective. For GFP intensity quantification, the background fluorescence of images was obtained from a remote reference region site and subtracted. GFP signal was identified and calculated from pixels with fluorescence values exceeding the mean background by three standard deviations. To evaluate the effect of doxorubicin, a region of interest (ROI) with 500 x 1300 μm size at the core of each injection was selected for calculation of GFP intensity. For cell number counting, stack images of 10-μm depth were acquired on Nikon TiE-A1plus confocal laser scanning microscope using a 40x/1.3 NA objective. Cells were identified with antibodies identifying cell-type specific marker, NeuN for total neurons, GFAP for astroglia, and Iba1 for microglia. Cell counting was performed manually or automatically using ImageJ (National Institutes of Health).

For neural circuit interrogation in macaque monkey, the brain was prepared for histological procedures according to previously procedures (Markov et al., 2011). Cryoprotection was performed with glycerol gradient perfusions as well as subsequent dehydration with 20% glycerol in PBS. The whole brain was cut into 40-μm-thick coronal sections symmetrically and 1 in 3 sections were taken for imaging and examination. Fluorescence images of three channels (DAPI, EGFP and Cy3) were obtained with ZEISS Axio Scan Z1 fluorescence microscope using a 10x objective. Area parcellation of LGN, V1, V2, V4, V5/MT and other brain regions was performed according to the MRI and histology atlas of rhesus monkey brain (Saleem and Logothetis, 2007), and tdTomato-labelled cells attributed to each area were identified and counted across sections taken every 480 μm manually. For LGN, the sampling interval was reduced to 120 μm and confocal images of 5-μm thickness were taken, with tdTomato-labelled cell bodies of red color counted manually. Pictures were stitched together with Adobe Illustrator software.

Two-photon calcium imaging

Mice were anaesthetized by 0.7~1.0% isoflurane via respiration and fixed with the implanted headplate. Body temperature was maintained at about 37°C with a heating pad, and animal state was monitored using an infrared camera. Images were acquired within an ROI (1024 x 1024 pixels) with a commercial two-photon microscope (Thorlabs) which was controlled by ThorImage software, via a 16× objective (NA = 0.8, Nikon). GCaMP6s-based Ca^{2+}

signal was excited with 910-nm wavelength that generated via a mode-locked Ti:sapphire laser (Mai Tai DeepSee, Spectra physics), and collected with filter 525/50. Visual stimuli were generated with the Psychtoolbox for MATLAB and presented monocularly on a 17-inch LCD monitor (Lenove) at a distance of 15 cm in front of the animal. Sinusoidal gratings (contrast = 1; spatial frequency = 0.05 cycle/degree; temporal frequency = 2 cycle/second) were displayed for 3 seconds and drifted at eight directions (0°, 45°, 90°, 135°, 180°, 225°, 270°, 315°) randomly, five repeats per condition. For each condition, images were captured at a frame rate of 7.8 Hz over a period of 8 seconds, including 1 second before stimuli onset. Before experiment, baseline fluorescence was collected for 200 frames without visual stimuli and treated as an indicator of GCaMP6s expression.

Images obtained in our experiment were analyzed with ImageJ (National Institutes of Health) and Matlab (Mathworks). For correcting lateral motion in the imaging data, a rigid-body transformation-based frame-by-frame alignment was applied by using Turboreg plugin (ImageJ software). Cells were identified on the basis of cross-trial variability calculation and manually modified by empirically handed labeling according to the size, shape, and brightness. Fluorescence changes with time of individual cells were extracted by averaging pixel intensity values within each cell in each frame. The fluorescence intensity change (ΔF) evoked by each stimulus (stimulus duration, 3s) was normalized by the pre-stimulus baseline fluorescence (F, 1s). For each stimulus, the mean change in fluorescence (ΔF/F) was calculated by averaging responses to all trials for each stimulus condition. Cells showing significant differences in the fluorescence intensity signals observed during baseline vs. stimulus-presentation periods ($P < 0.05$, ANOVA) were defined as "responsive cells". The response strength was determined as the maximal (ΔF/F) across all the stimulus conditions. The orientation selectivity index (OSI) was defined as (1-Var(θ)), where Var(θ) is the circular variance of the responses to the tested directions.

TUNEL assay

The TUNEL assay was performed according to the manufacturer's instructions (Beyotime technology, Shanghai). Briefly, brain sections fixed with 4% paraformaldehyde and permeabilized with 0.3% Triton X-100 were incubated with recombinant termination deoxynucleotidyltransferase (rTdT) for 1 hour at 37℃. The fragmented DNA was labeled at the ends with Cy3-conjugated dUTP to yield red-stained nuclei, indicative of an apoptotic cell. Positive control samples were pretreated with DNase I before TUNEL staining.

Behavior test

An 'open field' test was conducted according to previously described procedures (Seibenhener and Wooten, 2015). In short, after an 30 minutes acclimation, mice were placed individually in the middle of a 40 x 40 cm open field chamber and allowed to explore freely for 15 minutes. Throughout this period the movement trajectory of the mouse was tracked with a video camera controlled by the EthoVision XT software. Total distance traveled, mean velocity, and time in movement were calculated as measures of locomotor activity.

Statistics

Statistical analysis was performed with GraphPad Prism 7 and MATLAB. A test for normality was applied before statistical comparison. If the data conformed to a normal distribution, an unpaired two-tail Student's t-test or one-way ANOVA followed by post–hoc Tukey Kramer correction were used for comparisons between different groups; if not, the Wilcoxon rank sum test was used. For comparison of transgene expression at three days (Fig. 1F), both the control group (n = 6) and doxorubicin-treated group (n = 6) had one injection excluded from subsequent analysis

upon failure of immunohistochemical detection. For Figures 3C, 4B, 4C, 4E and 5B, data distribution was assumed to be normal and an unpaired, two-tail student's t-test was used. All data are presented as means ± SEM, and statistical test, n numbers of each group and p values are reported in figure legends. Threshold p values were computed for significance levels: *$p < 0.05$, **$p < 0.01$,***$p < 0.001$.

Acknowledgments

This work was supported by the Strategic Priority Research Program of Chinese Academy of Sciences, Grant No. XDB 32060200 to W.W.; Shanghai Municipal Science and Technology Major Project, Grant No. 2018SHZDZX05 to W.W.; National Natural Science Foundation of China Grant No. 31861143032; National Key Research and Development Program of China 2020YFA0112703

Author contributions

W.W. designed research; HL.G., NN.Y., ZM.S., C.T., performed research; S.S., LL.Q, YL.L, I.M.A., SH.Z, JH.W., and G.Y. contributed analytic tools; HL.G. analyzed data; HL.G., S.S., and W.W. wrote the paper.

Competing interests

The authors declare no competing interests.

References

Alexander, I.E., Russell, D.W., and Miller, A.D. (1994). DNA-damaging agents greatly increase the transduction of nondividing cells by adeno-associated virus vectors. J Virol *68*, 8282-8287.

Alli, S., Figueiredo, C.A., Golbourn, B., Sabha, N., Wu, M.Y., Bondoc, A., Luck, A., Coluccia, D., Maslink, C., Smith, C.*, et al.* (2018). Brainstem blood brain barrier disruption using focused ultrasound: A demonstration of feasibility and enhanced doxorubicin delivery. J Control Release *281*, 29-41.

Angelucci, A., and Sainsbury, K. (2006). Contribution of feedforward thalamic afferents and corticogeniculate feedback to the spatial summation area of macaque V1 and LGN. J Comp Neurol *498*, 330-351.

Atasoy, D., Aponte, Y., Su, H.H., and Sternson, S.M. (2008). A FLEX switch targets Channelrhodopsin-2 to multiple cell types for imaging and long-range circuit mapping. The Journal of neuroscience : the official journal of the Society for Neuroscience *28*, 7025-7030.

Betley, J.N., and Sternson, S.M. (2011). Adeno-associated viral vectors for mapping, monitoring, and manipulating neural circuits. Human gene therapy *22*, 669-677.

Bigotte, L., and Olsson, Y. (1982). Retrograde transport of doxorubicin (adriamycin) in peripheral nerves of mice. Neurosci Lett *32*, 217-221.

Broekman, M.L.D., Comer, L.A., Hyman, B.T., and Siena-Esteves, M. (2006). Adeno-associated virus vectors serotyped with AAV8 capsid are more efficient than AAV-1 or-2 serotypes for widespread gene delivery to the neonatal mouse brain. Neuroscience *138*, 501-510.

Chan, K.Y., Jang, M.J., Yoo, B.B., Greenbaum, A., Ravi, N., Wu, W.L., Sanchez-Guardado, L., Lois, C., Mazmanian, S.K., Deverman, B.E.*, et al.* (2017). Engineered AAVs for efficient noninvasive gene delivery to the central and peripheral nervous systems. Nat Neurosci *20*, 1172-1179.

Choi, V.W., McCarty, D.M., and Samulski, R.J. (2006). Host cell DNA repair pathways in adeno-associated viral genome processing. J Virol *80*, 10346-10356.

Craig, A.J., and Housley, G.D. (2016). Evaluation of Gene Therapy as an Intervention Strategy to Treat Brain Injury from Stroke. Front Mol Neurosci *9*.

Cruz-Martin, A., El-Danaf, R.N., Osakada, F., Sriram, B., Dhande, O.S., Nguyen, P.L., Callaway, E.M., Ghosh, A., and Huberman, A.D. (2014). A dedicated circuit links direction-selective retinal ganglion cells to the primary visual cortex. Nature *507*, 358-361.

Dayton, R.D., Wang, D.B., and Klein, R.L. (2012). The advent of AAV9 expands applications for brain and spinal cord gene delivery. Expert Opin Biol Th *12*, 757-766.

Deverman, B.E., Pravdo, P.L., Simpson, B.P., Kumar, S.R., Chan, K.Y., Banerjee, A., Wu, W.L., Yang, B., Huber, N., Pasca, S.P.*, et al.* (2016). Cre-dependent selection yields AAV variants for widespread gene transfer to the adult brain. Nat Biotechnol *34*, 204-209.

Diester, I., Kaufman, M.T., Mogri, M., Pashaie, R., Goo, W., Yizhar, O., Ramakrishnan, C., Deisseroth, K., and Shenoy, K.V. (2011). An optogenetic toolbox designed for primates. Nature Neuroscience *14*, 387-397.
Ferrari, F.K., Samulski, T., Shenk, T., and Samulski, R.J. (1996). Second-strand synthesis is a rate-limiting step for efficient transduction by recombinant adeno-associated virus vectors. J Virol *70*, 3227-3234.
Fisher, K.J., Gao, G.P., Weitzman, M.D., DeMatteo, R., Burda, J.F., and Wilson, J.M. (1996). Transduction with recombinant adeno-associated virus for gene therapy is limited by leading-strand synthesis. J Virol *70*, 520-532.
Foust, K.D., Nurre, E., Montgomery, C.L., Hernandez, A., Chan, C.M., and Kaspar, B.K. (2009). Intravascular AAV9 preferentially targets neonatal neurons and adult astrocytes. Nat Biotechnol *27*, 59-65.
Fu, H.Y., and McCarty, D.M. (2016). Crossing the blood-brain-barrier with viral vectors. Curr Opin Virol *21*, 87-92.
Gao, G.P., Alvira, M.R., Wang, L., Calcedo, R., Johnston, J., and Wilson, J.M. (2002). Novel adeno-associated viruses from rhesus monkeys as vectors for human gene therapy. Proceedings of the National Academy of Sciences of the United States of America *99*, 11854-11859.
Gilkes, J.A., Bloom, M.D., and Heldermon, C.D. (2016). Preferred transduction with AAV8 and AAV9 via thalamic administration in the MPS IIIB model: A comparison of four rAAV serotypes. Molec Genet Metab Rep *6*, 48-54.
Hadaczek, P., Eberling, J.L., Pivirotto, P., Bringas, J., Forsayeth, J., and Bankiewicz, K.S. (2010). Eight years of clinical improvement in MPTP-lesioned primates after gene therapy with AAV2-hAADC. Molecular Therapy *18*, 1458-1461.
Harbison, C.E., Chiorini, J.A., and Parrish, C.R. (2008). The parvovirus capsid odyssey: from the cell sur face to the nucleus. Trends Microbiol *16*, 208-214.
Hudry, E., and Vandenberghe, L.H. (2019). Therapeutic AAV Gene Transfer to the Nervous System: A Clinical Reality. Neuron *101*, 839-862.
Hwu, W.L., Muramatsu, S., Tseng, S.H., Tzen, K.Y., Lee, N.C., Chien, Y.H., Snyder, R.O., Byrne, B.J., Tai, C.H., and Wu, R.M. (2012). Gene therapy for aromatic L-amino acid decarboxylase deficiency. Sci Transl Med *4*, 134ra161.
Ju, N.S., Jiang, R.D., Macknik, S.L., Martinez-Conde, S., and Tang, S.M. (2018). Long-term all-optical interrogation of cortical neurons in awake-behaving nonhuman primates. PLoS Biol *16*, 17.
Kanazawa, T., Urabe, M., Mizukami, H., Okada, T., Kume, A., Nishino, H., Monahan, J., Kitamura, K., Ichimura, K., and Ozawa, K. (2001). Gamma-rays enhance rAAV-mediated transgene expression and cytocidal effect of AAV-HSVtk/ganciclovir on cancer cells. Cancer gene therapy *8*, 99-106.
Kennedy, H., and Bullier, J. (1985). A double-labeling investigation of the afferent connectivity to cortical areas V1 and V2 of the macaque monkey. The Journal of neuroscience : the official journal of the Society for Neuroscience *5*, 2815-2830.
Koda, L.Y., and Van der Kooy, D. (1983). Doxorubicin: a fluorescent neurotoxin retrogradely transported in the central nervous system. Neuroscience Letters *36*, 1-8.
Krol, A., and Feng, G.P. (2018). Windows of opportunity: timing in neurodevelopmental disorders. Curr Opin Neurobiol *48*, 59-63.
Lu, H., Wang, Y., He, X., Yuan, F., Lin, X., Xie, B., Tang, G., Huang, J., Tang, Y., Jin, K.*, et al.* (2012). Netrin-1 hyperexpression in mouse brain promotes angiogenesis and long-term neurological recovery after transient focal ischemia. Stroke *43*, 838-843.
Maes, M.E., Colombo, G., Schulz, R., and Siegert, S. (2019). Targeting microglia with lentivirus and AAV: Recent advances and remaining challenges. Neuroscience Letters *707*, 134310.
Maheshri, N., Koerber, J.T., Kaspar, B.K., and Schaffer, D.V. (2006). Directed evolution of adeno-associated virus yields enhanced gene delivery vectors. Nat Biotechnol *24*, 198-204.
Manno, C.S., Arruda, V.R., Pierce, G.F., Glader, B., Ragni, M., Rasko, J., Ozelo, M.C., Hoots, K., Blatt, P., Konkle, B.*, et al.* (2006). Successful transduction of liver in hemophilia by AAV-Factor IX and limitations imposed by the host immune response (vol 12, pg 342, 2006). Nature Medicine *12*, 592-592.
Markov, N.T., Misery, P., Falchier, A., Lamy, C., Vezoli, J., Quilodran, R., Gariel, M.A., Giroud, P., Ercsey-Ravasz, M., Pilaz, L.J.*, et al.* (2011). Weight consistency specifies regularities of macaque cortical networks. Cereb Cortex *21*, 1254-1272.
Masamizu, Y., Okada, T., Ishibashi, H., Takeda, S., Yuasa, S., and Nakahara, K. (2010). Efficient gene transfer into neurons in monkey brain by adeno-associated virus 8. Neuroreport *21*, 447-451.
McCarty, D.M., Fu, H., Monahan, P.E., Toulson, C.E., Naik, P., and Samulski, R.J. (2003). Adeno-associated virus terminal repeat (TR) mutant generates self-complementary vectors to overcome the rate-limiting step to transduction in vivo. Gene Ther *10*, 2112-2118.
Mehta, A.M., Sonabend, A.M., and Bruce, J.N. (2017). Convection-Enhanced Delivery. Neurotherapeutics *14*, 358-371.
Mendell, J.R., Al-Zaidy, S., Shell, R., Arnold, W.D., Rodino-Klapac, L.R., Prior, T.W., Lowes, L., Alfano, L., Berry, K., Church, K.*, et al.* (2017). Single-Dose Gene-Replacement Therapy for Spinal Muscular Atrophy. New England Journal of Medicine *377*, 1713-1722.
Mingozzi, F., Maus, M.V., Hui, D.J., Sabatino, D.E., Murphy, S.L., Rasko, J.E., Ragni, M.V., Manno, C.S., Sommer, J., Jiang, H.*, et al.* (2007). CD8(+) T-cell responses to adeno-associated virus capsid in humans. Nat Med *13*, 419-422.
Mross, K., Maessen, P., Vandervijgh, W.J.F., Gall, H., Boven, E., and Pinedo, H.M. (1988). Pharmacokinetics and Metabolism of Epidoxorubicin and Doxorubicin in Humans. J Clin Oncol *6*, 517-526.
Nicolson, S.C., Li, C.W., Hirsch, M.L., Setola, V., and Samulski, R.J. (2016). Identification and Validation of Small Molecules That Enhance Recombinant Adeno-associated Virus Transduction following High-Throughput Screens. J Virol *90*, 7019-7031.
Parekh, R., and Ascoli, G.A. (2013). Neuronal morphology goes digital: a research hub for cellular and system neuroscience. Neuron *77*, 1017-1038.

Peel, A.L., Zolotukhin, S., Schrimsher, G.W., Muzyczka, N., and Reier, P.J. (1997). Efficient transduction of green fluorescent protein in spinal cord neurons using adeno-associated virus vectors containing cell type-specific promoters. Gene Ther *4*, 16-24.
Perkel, D.J., Bullier, J., and Kennedy, H. (1986). Topography of the afferent connectivity of area 17 in the macaque monkey: a double-labelling study. J Comp Neurol *253*, 374-402.
Rabinowitz, J.E., Bowles, D.E., Faust, S.M., Ledford, J.G., Cunningham, S.E., and Samulski, R.J. (2004). Cross-dressing the virion: the transcapsidation of adeno-associated virus serotypes functionally defines subgroups. J Virol *78*, 4421-4432.
Ran, F.A., Cong, L., Yan, W.X., Scott, D.A., Gootenberg, J.S., Kriz, A.J., Zetsche, B., Shalem, O., Wu, X.B., Makarova, K.S.*, et al.* (2015). In vivo genome editing using Staphylococcus aureus Cas9. Nature *520*, 186-U198.
Russell, D.W., Alexander, I.E., and Miller, A.D. (1995). DNA synthesis and topoisomerase inhibitors increase transduction by adeno-associated virus vectors. Proceedings of the National Academy of Sciences of the United States of America *92*, 5719-5723.
Saleem, K.S., and Logothetis, N. (2007). A combined MRI and histology atlas of the rhesus monkey brain in stereotaxic coordinates (London ; Burlington, MA: Academic).
Sauter, K.A.D., Wood, L.J., Wong, J., Iordanov, M., and Magun, B.E. (2011). Doxorubicin and daunorubicin induce processing and release of interleukin-1 beta through activation of the NLRP3 inflammasome. Cancer Biol Ther *11*, 1008-1016.
Scanziani, M., and Hausser, M. (2009). Electrophysiology in the age of light. Nature *461*, 930-939.
Seibenhener, M.L., and Wooten, M.C. (2015). Use of the Open Field Maze to measure locomotor and anxiety-like behavior in mice. J Vis Exp.
Shimazaki, K., Urabe, M., Monahan, J., Ozawa, K., and Kawai, N. (2000). Adeno-associated virus vector-mediated bcl-2 gene transfer info post-ischemic gerbil brain in vivo: prospects for gene therapy of ischemia-induced neuronal death. Gene Ther *7*, 1244-1249.
Sishi, B.J.N., Loos, B., van Rooyen, J., and Engelbrecht, A.M. (2013). Doxorubicin induces protein ubiquitination and inhibits proteasome activity during cardiotoxicity. Toxicology *309*, 23-29.
Srivastava, A. (2016). In vivo tissue-tropism of adeno-associated viral vectors. Curr Opin Virol *21*, 75-80.
Tacar, O., Sriamornsak, P., and Dass, C.R. (2013). Doxorubicin: an update on anticancer molecular action, toxicity and novel drug delivery systems. The Journal of pharmacy and pharmacology *65*, 157-170.
Tervo, D.G.R., Hwang, B.Y., Viswanathan, S., Gaj, T., Lavzin, M., Ritola, K.D., Lindo, S., Michael, S., Kuleshova, E., Ojala, D.*, et al.* (2016). A Designer AAV Variant Permits Efficient Retrograde Access to Projection Neurons. Neuron *92*, 372-382.
Tian, L., Hires, S.A., Mao, T., Huber, D., Chiappe, M.E., Chalasani, S.H., Petreanu, L., Akerboom, J., McKinney, S.A., Schreiter, E.R.*, et al.* (2009). Imaging neural activity in worms, flies and mice with improved GCaMP calcium indicators. Nature methods *6*, 875-881.
Vite, C.H., Passini, M.A., Haskins, M.E., and Wolfe, J.H. (2003). Adeno-associated virus vector-mediated transduction in the cat brain. Gene Ther *10*, 1874-1881.
Wang, D., Tai, P.W.L., and Gao, G.P. (2019). Adeno-associated virus vector as a platform for gene therapy delivery. Nature Reviews Drug Discovery *18*, 358-378.
Watakabe, A., Ohtsuka, M., Kinoshita, M., Takaji, M., Isa, K., Mizukami, H., Ozawa, K., Isa, T., and Yamamori, T. (2015). Comparative analyses of adeno-associated viral vector serotypes 1, 2, 5, 8 and 9 in marmoset, mouse and macaque cerebral cortex. Neurosci Res *93*, 144-157.
Weller, R.E., and Kaas, J.H. (1983). Retinotopic pattern of connections of area 17 with visual areas V-II and MT in macaque monkeys. J Comp Neurol *220*, 253-279.
Yan, Z.Y., Zak, R., Zhang, Y.L., Ding, W., Godwin, S., Munson, K., Peluso, R., and Engelhardt, J.F. (2004). Distinct classes of proteasome-modulating agents cooperatively augment recombinant adeno-associated virus type 2 and type 5-mediated transduction from the apical surfaces of human airway epithelia. J Virol *78*, 2863-2874.
Yang, L., Jiang, J., Drouin, L.M., Agbandje-McKenna, M., Chen, C., Qiao, C., Pu, D., Hu, X., Wang, D.Z., Li, J.*, et al.* (2009). A myocardium tropic adeno-associated virus (AAV) evolved by DNA shuffling and in vivo selection. Proceedings of the National Academy of Sciences of the United States of America *106*, 3946-3951.
Zhang, S., Xu, M., Chang, W.-C., Ma, C., Hoang Do, J.P., Jeong, D., Lei, T., Fan, J.L., and Dan, Y. (2016). Organization of long-range inputs and outputs of frontal cortex for top-down control. Nature Neuroscience *19*, 1733-1742.
Zhang, S.H., Wu, J.H., Wu, X.B., Xu, P., Tian, Y.H., Yi, M.Y., Liu, X.J., Dong, X.Y., Wolf, F., Li, C.Y.*, et al.* (2012). Enhancement of rAAV2-Mediated Transgene Expression in Retina Cells In Vitro and In Vivo by Coadministration of Low-Dose Chemotherapeutic Drugs. Invest Ophth Vis Sci *53*, 2675-2684.
Zhang, T., Hu, J., Ding, W., and Wang, X.M. (2009). Doxorubicin augments rAAV-2 transduction in rat neuronal cells. Neurochem Int *55*, 521-528.
Zhong, L., Li, B., Mah, C.S., Govindasamy, L., Agbandje-McKenna, M., Cooper, M., Herzog, R.W., Zolotukhin, I., Warrington, K.H., Jr., Weigel-Van Aken, K.A.*, et al.* (2008). Next generation of adeno-associated virus 2 vectors: point mutations in tyrosines lead to high-efficiency transduction at lower doses. Proceedings of the National Academy of Sciences of the United States of America *105*, 7827-7832.

Supplementary figures

Figure 1–figure supplement 1

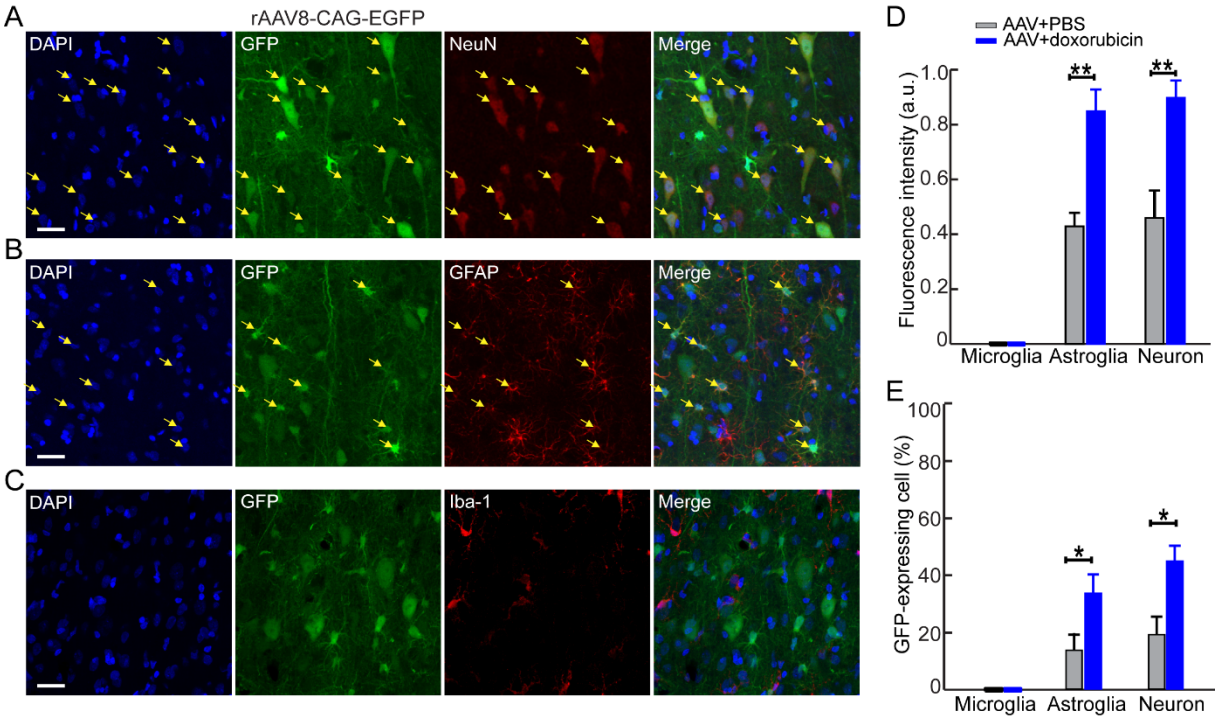

Doxorubicin promotes rAAV8 transduction in neurons without impact on its cellular tropism. (**A-C**) Phenotype of transduced neurons, astroglia and microglia identified with NeuN, GFAP and Iba-1 staining, respectively. Yellow arrows indicate the co-localization of GFP and cell type-specific marker. DAPI, nuclear marker; NeuN, marker of neuron; GFAP, marker of astroglia; Iba1, marker of microglia. Scale bar, 25 µm (**D**) Quantification of GFP intensity in transduced cells in the control and doxorubicin-treated cases. Neuron, p = 0.0061; Astrocyte, p = 0.0068. Unpaired two-tailed t-test. (**E**) Quantification of the percentage of transduced cells in two groups. Neuron, Neuron: 41 ± 4% vs 21 ± 6%; p = 0.038; Astrocyte: 32 ± 6% vs 14 ± 4%; p = 0. 033.Unpaired two-tailed t-test. For quantification in **D** and **E**, n = 4 injections from 4 cats, mean ± SEM, *p <0.05, **p <0.01,

Figure 2–figure supplement 1

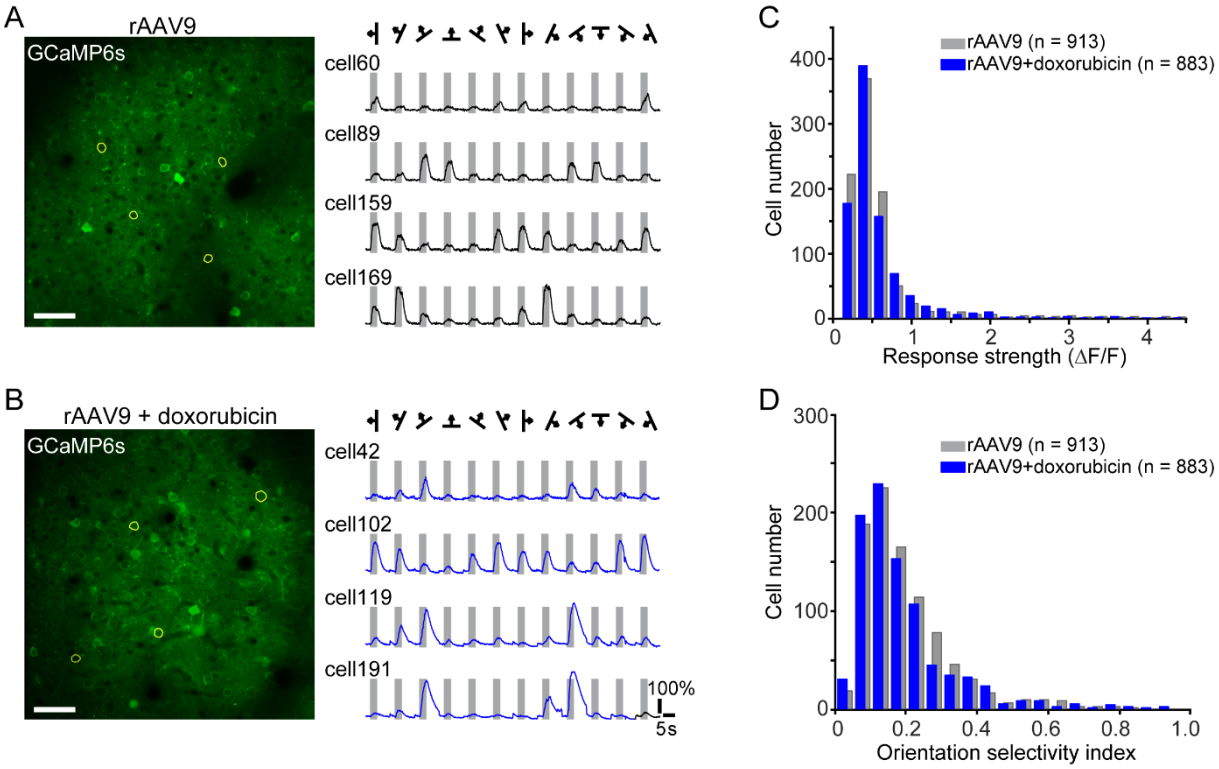

***In vivo* two-photon calcium imaging reveals little functional difference under experiment conditions**

(**A-B**) *In vivo* two-photon image of Ca^{2+} fluorescence from the control (~30 day post-injection) and doxorubicin-treated mice (~15 day post-injection) with comparable expression level of GCaMP6s. Mean fluorescence changes (ΔF/F) of sampled cells (marked by yellow circles) evoked by drifting sine-wave grating stimuli. Scale bar, 50 μm. (**C**) Histograms of cell response strength distributions for all responsive cells recorded from the two mouse groups (rAAV9, n = 913 cells; rAAV9-plus-doxorubicn, n = 883 cells). Median of control group 0.43, median of doxorubicin-treated group 0.42; p = 0.25, Wilcoxon rank-sum test. (**D**) Histograms of the orientation-selectivity index distributions for all responsive cells recorded from the two groups (rAAV9, n = 913 cells; rAAV9-plus-doxorubicn, n = 883 cells). Median of control group 0.132, median of doxorubicin-treated group 0.122; p = 0.06, Wilcoxon rank-sum test. In **C-D**, 5 ROIs per group.

Figure 5–figure supplement 1

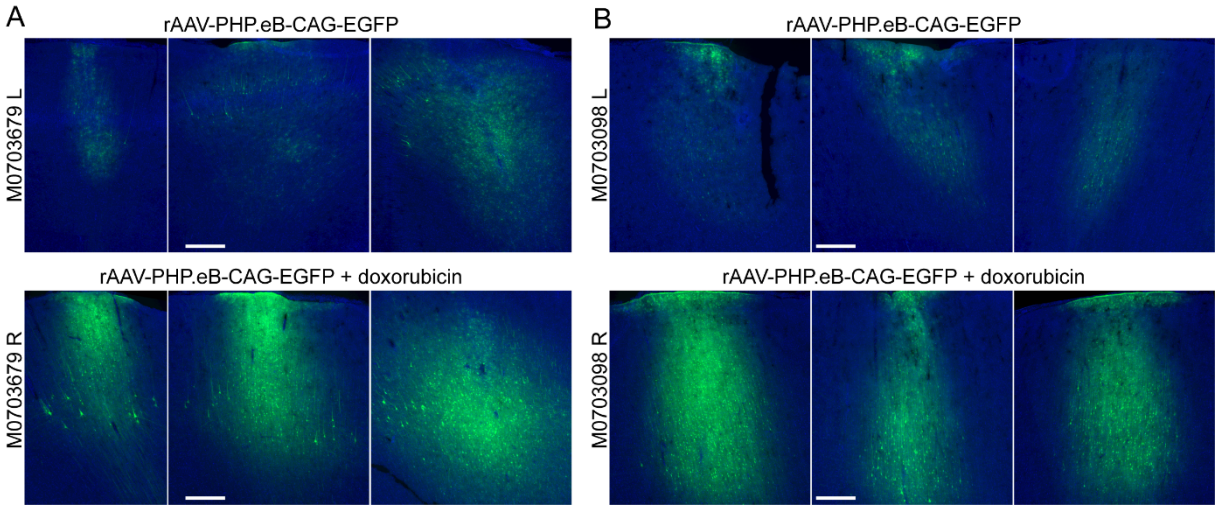

Doxorubicin enhances rAAV-PHP.eB transduction in the motor cortex of macaque monkeys

(**A**) Fluorescence images from three injections of the control and doxorubicin-treated group in M0703679, respectively. rAAV-PHP.eB-CAG-EGFP vector was administered into the left and right motor cortices with or without doxorubicin (10 μg/ml), respectively. GFP intensities were assessed with histological techniques seven days post-injection. (**B**) Similar injections' results from M0703098. Scale bar, 500 μm.

Figure 6–figure supplement 1

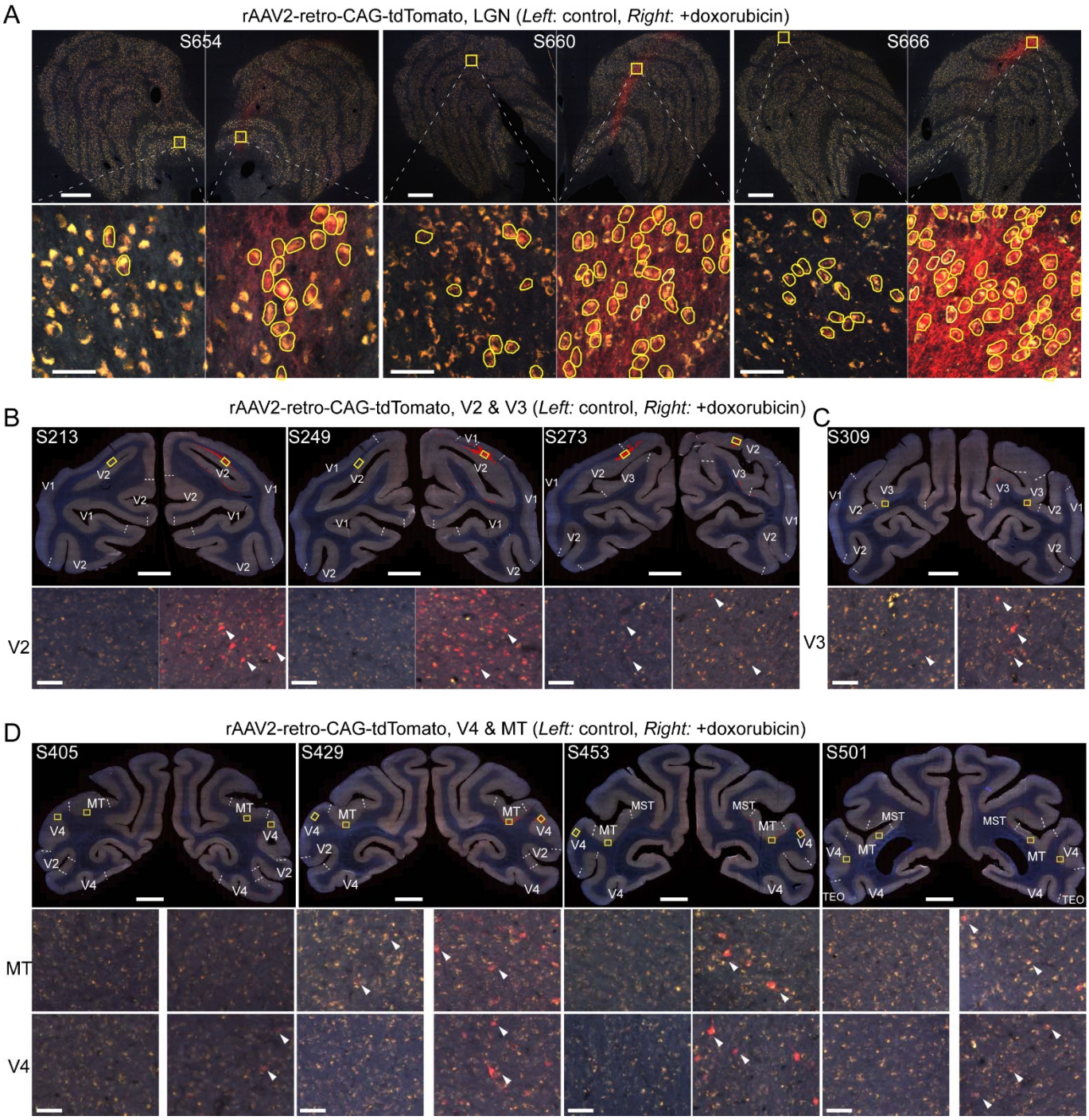

Doxorubicin enhances rAAV2-retro-based transgene expression for neural circuit interrogation in the visual system of macaque M022

(A) Schematic representation of LGN sections from hemispheres injected with vector alone (*left*) or vector coupled with doxorubicin (*right*). Upper panel: whole coronal image of LGN in different sections (S654, S660 and S666); scale bar, 500 μm. Lower panel: transduced neurons from the above ROIs are marked with white circles; scale bar, 50 μm. **(B)** Schematic representation of V2 sections from the left and right hemisphere. (**C**) Schematic representation of V3 from the left and right hemisphere. **(D)** Representative images of V4 and MT from the left and right hemisphere. Upper panels in **B, C** and **D** show whole coronal images with transduced cells marked by red dots; scale bar, 5000 μm. Lower panels (middle and bottom panels in **D**) show transduced neurons from ROIs (boxed in the upper panel) of V2, V3, V4 and MT marked by white arrowheads; scale bar, 50 μm.